UNIVERSITY OF OKLAHOMA

GRADUATE COLLEGE

GLOBAL ANALYSIS OF CHARACTERISTICS OF TROPICAL EASTERLY WAVES AND RELATED PRECIPITATION

A THESIS

SUBMITTED TO THE GRADUATE FACULTY

in partial fulfillment of the requirements for the

Degree of

MASTER OF SCIENCE IN METEOROLOGY

By

MARGARET ANNE HOLLIS
Norman, Oklahoma
2021

GLOBAL ANALYSIS OF CHARACTERISTICS OF TROPICAL EASTERLY WAVES AND RELATED PRECIPITATION

A THESIS APPROVED FOR THE
SCHOOL OF METEOROLOGY

BY THE COMMITTEE CONSISTING OF

Dr. Elinor Martin, Chair

Dr. Naoko Sakaeda

Dr. Pierre Kirstetter

Dedication

To everyone who did part or all their Master's Thesis in a pandemic. The world may have ground to a halt and tried to make it hard to get work done, but we did it anyways.

Acknowledgments

There are a lot of thanks that go to a lot of people over the course of my thesis. First and foremost, I'd like to thank my advisor, Dr. Elinor Martin, for her support, guidance, and advice throughout the entire course of my Master's research. Many thanks also go to our collaborators in researching tropical easterly waves, Carrie Lewis-Merritt, Dr. Justin Stachnik, and Dr. Rachel McCrary, who asked great questions about my preliminary results during our group meetings. Additional thanks go to my committee members, Dr. Naoko Sakaeda and Dr. Pierre Kirstetter, for their feedback on my thesis.

A huge thanks to my peers in the rest of the Climate Variability and Change group, the Weather and Climate Interactions Group, and Office 5700. While we haven't all been in one place in a while, you all made me feel welcome when I moved to start grad school and helped me get started with research. I also greatly appreciate the feedback on my various presentations, which has helped me refine my explanation of what a tropical easterly wave is and what my results mean.

Thank you to NASA's Precipitation Measurement Mission for funding this research.

And finally, thank you to my family and friends for all of your support, memes, and pet pictures. The last two and a half years haven't been easy by any means. Having your support and humor has been a huge part of how I got through when my code was broken and my plots looked terrible. I'm glad I didn't scare anyone away by talking about waves.

Table of Contents

List Of Tables

List Of Figures

Abstract

Tropical easterly waves (TEWs) are important components of tropical convection and precipitation, especially in summer months. The most well-documented TEWs are African easterly waves (AEWs), which have been linked with rainfall variability and mesoscale convective systems in the Sahel region, as well as Atlantic tropical cyclone activity. TEWs in the Caribbean and eastern Pacific have also been shown to contribute to up to half of summertime rainfall in those regions. However, no global study of TEWs and their related precipitation exists. To fill this gap, we have created a global database of TEW tracks at both 850 and 700 hPa by using TRACK to identify regions of cyclonic curvature vorticity (CV) that meet thresholds for CV intensity, propagation direction and distance, and track length. In this database, we have identified 38723 TEW tracks throughout the entire tropics, with 14447 tracks at 850 hPa and 24276 tracks at 700 hPa. Globally and for each combination of level and hemisphere, the TEWs we identified have an average phase speed of 7.5 ms^{-1} and average propagation distance of 3000 km. In both hemispheres, there is a strong seasonal cycle, as well as interannual variability in TEW activity. Using these tracks and IMERG precipitation data, we found that TEWs can be associated with 20-30% of the total annual rainfall in regions with increased TEW activity and that TEWs with greater vertical coherence have more precipitation in the 500 km radius around the CV center. This global study on TEW activity and precipitation gives a global context to TEW behavior and importance across the tropics. In the future, these TEW tracks and their associated precipitation can also be used for additional studies on TEW lifecycles, interannual variability, and regional comparisons.

Chapter 1

Introduction and Background

Tropical easterly waves (TEWs) are synoptic-scale waves that occur in the tropics and propagate from east to west. The most represented subset of TEWs in literature, African Easterly Waves (AEWs) are well-documented as having wavelengths of 2000-4000 km, phase speeds of 6-8 ms^{-1}, and periods of 2-5 days (Carlson 1969; Reed et al. 1977; Burpee 1972). AEWs originate in the tropical latitudes of Africa and propagate westward into the Atlantic Ocean. The limited current studies on westward-propagating synoptic-scale waves in other regions, mainly using reanalysis data, have returned similar values for various other regions (e.g. Schreck et al. 2011; Fukutomi 2019). Many TEWs are associated with increased cloudiness and convection, but some TEWs may be dry, identifiable instead by streamlines, surface pressure, or other dynamical fields (e.g., Carlson 1969; Thorncroft and Hodges 2001). Wheeler and Kiladis (1999) also identified TEWs in a wavenumber-frequency analysis of the tropics using outgoing longwave radiation as a proxy for convection.

The convection associated with TEWs and the frequency of TEWs can impact the rainfall in regions across the tropics. Studies such as Moron et al. (2008); Engel et al. (2017) have linked AEWs with weather patterns and extreme rainfall events in western Africa. Beyond Africa, Dominguez et al. (2020) found that TEWs that reach the Caribbean and northern South America contribute to up to 50% of summertime rainfall in parts of the region. Further west, Ladwig and Stensrud (2009) also showed that TEWs may influence the intensity and domain of the North American Monsoon. TEW impacts also sometimes extend into the

midlatitudes by way of tropical cyclones (TCs), as some TEWs serve as precursor disturbances to TCs (Landsea and Gray 1992; Pasch and Avila 1994; Schreck et al. 2011).

Most existing studies on TEWs focus on one or two regions, often Africa and the North Atlantic Ocean or the eastern North Pacific Ocean. Even most larger climatologies only consider a limited domain, such as Belanger et al. (2016), which only covers the western hemisphere. Development of a global climatology of TEWs using consistent definitions provides the opportunity to compare the entire global tropics, including less-studied regions that may lack robust, regular TEW activity. This TEW climatology then becomes a valuable tool for studying precipitation across the tropics and the role TEWs play in tropical precipitation.

1.1 Background on Tropical Easterly Waves

The vast majority of existing literature focuses on AEWs, with a secondary focus on TEWs in the eastern North Pacific Ocean. Within the limited literature on TEWs in other regions, there are many discrepancies in how waves are defined and identified. Especially in studies that identify waves in reanalysis data, it is difficult to compare studies because each study uses its own combination of identification variable(s), tracking method, and data source. This introduces challenges when trying to compare TEWs globally (Hurley and Boos 2015). While reanalyses have biases and may under-represent some phenomena, global reanalyses allow researchers to use a consistent data set and methods (Hodges et al. 2017). Hodges et al. (2017) in particular noted that in many cases lower strength TCs and their precursor disturbances, including TEWs, are often weaker in reanalyses than they were in observations.

Older literature on AEWs suggests that these waves form due to the combination of a reversal of the meridional isentropic potential vorticity gradient and the African easterly jet (AEJ) (e.g., Eliassen 1983; Burpee 1972; Charney and Stern 1962). In these studies, the

authors propose that AEWs develop because the instability criteria from Charney and Stern (1962) is met near the AEJ (Burpee 1972).

As computer models have advanced, simulation of the AEJ and the conditions surrounding the generation of AEWs has become possible. One such set of simulations, described in Hsieh and Cook (2005), studied the relationship between AEWs, the AEJ, and surface soil moisture over north Africa. Through variations on the initial conditions, the authors found that AEWs developed regardless of the presence of the AEJ. The AEWs in the simulations without the AEJ were smaller and had less convection associated with them than those in the simulations with the AEJ. This led the authors to conclude that the AEJ is not essential for AEW development, but is instead an important factor in modulating the strength of AEWs.

Many studies that focus on AEWs note two distinct areas of increased track density over Africa, a lower-level maximum located poleward of the AEJ at 850 hPa, and a mid-level maximum equatorward of the AEJ and strongest at 600-700 hPa (e.g., Thorncroft and Hodges 2001; Reed et al. 1988, Hopsch et al. 2007,). Reed et al. (1988), which used archived forecast and satellite imagery, identified these two primary source regions for AEWs in their study of the period spanning August-September 1985. This phenomenon has been observed in many studies since then, including studies using reanalysis data such as Thorncroft and Hodges (2001) as well as studies relying on models such as Hsieh and Cook (2005). The exact latitudes for these wave track vary between studies, but typical latitudes for southern track for AEWs range from 5-15°N, while typical latitudes extend poleward from 15°N and may be as far north as 30°N (Brannan and Martin 2019; Thorncroft and Hodges 2001).

In considering other regions where TEWs may occur, Dickinson and Molinari (2000) looked to Australia. Like Africa, Australia has a vast desert located poleward of equatorial ocean. To quantify the potential similarity between the two regions, the authors developed a climatology of the PV gradient for both north Africa and northern Australia. They found that the PV gradient over Australia was sufficient to meet the instability criteria from Charney

and Stern (1962). Despite this, when using bandpass filtered meridional winds and OLR, there was minimal evidence for the growth of disturbances along the region of the PV sign reversal over Australia.

In contrast with the bandpass filtering used in Dickinson and Molinari (2000), Berry et al. (2012) identified individual PV maxima to create individual tracks when developing their climatology of synoptic-scale disturbances in the Australian monsoon. Tracked on multiple isentropic levels, the authors found a distinct region of westward-propagating disturbances between 5°S and 20°S, near where Dickinson and Molinari (2000) identified the PV gradient. In an attempt to reconcile the differences of their study with Dickinson and Molinari (2000), Berry et al. (2012) performed the same tracking over west Africa to identify AEWs and found that systems in the Australian monsoon region, while having a similar average interval between disturbances, exhibit more variability in their periodicity than AEWs.

Regional studies also exist for the Caribbean and adjacent regions, as well as the eastern orth Pacific Ocean. Dominguez et al. (2020) tracked TEWs at three vertical levels for the North Atlantic Ocean and eastern North Pacific, identifying not only AEWs tracking across the Atlantic Ocean but also a large number of TEWs originating in the Pacific Ocean just west of Central America. This finding was consistent with an earlier study in the same region by Serra et al. (2010), which also identified a large peak in TEW activity west of Central America. In both of these studies, the preferred wave track region is along 10°N, some waves are tracked through the Caribbean, but many more are generated in the Pacific Ocean.

The limited overlap in domains between regions, as well discrepancies between regional studies like Dickinson and Molinari (2000) and Berry et al. (2012) highlight how different methods and assumptions can yield different results. With such widely varied results depending on the methods used and regions studied, any global discussion of TEWs need to be based on a consistent, global study, rather than comparing the results in different regions.

Regional studies are not without use, however. These studies may serve as a point of comparison for larger regional studies, as well as global studies. For example, the climatology described in Hurley and Boos (2015) is a global climatology of monsoon low-pressure systems, which includes many TEWs. With an interest on monsoon systems, the authors used existing databases of Indian monsoon systems to compare their results and lend confidence to their methods.

The Hurley and Boos (2015) study, in line with the goals of the study, uses criteria that may exclude some TEWs, and also includes tropical waves that do not have a significant easterly component to their motion. Nonetheless, it is a useful point of comparison for both TEW activity and precipitation. The Hurley and Boos (2015) climatology, which focused on monsoon low-pressure systems, identified particular areas of activity across the global tropics, with weak monsoon lows identified across Asia, Africa, the Americas, and Australia.

Another large study by Belanger et al. (2016) focused on TEWs in the western hemisphere. The authors applied their methods to four reanalysis datasets. In their results, the authors showed peaks in TEW activity not only across the North Atlantic AEW track region and the north east Pacific, but additional peaks in the southern hemisphere. These additional peaks, downstream of Africa and over and downstream of South America, were between 5-25°S. For all of the maxima identified by Belanger et al. (2016), the magnitude varies by dataset, underlining the complications in comparing studies using different data sources.

From the smaller regional studies and larger hemispheric and global studies, such as those discussed above, it is reasonable to conclude that TEWs occur across and are important to not only north Africa and the North Atlantic basin, but the entire global tropics. A global climatology of TEWs would help to connect these studies further, and could serve as a starting point for further research.

1.2 Background on Tropical Precipitation

The convection associated with TEWs is an important driver for rainfall in regions where they occur (e.g., Fink and Reiner 2003; Dominguez et al. 2020; Berry et al. 2012). Studies have attempted to assess the contributions TEWs make to rainfall in the tropics through varying means. Thorncroft and Hodges (2001) found that a simple linear correlation between the number of AEWs passing through a box along the west African coastline and Sahel rainfall was weak, with a correlation coefficient of 0.33 significant only at the 85% level. Therefore, many studies relate TEWs with other features of a region's weather, such as the study by Fink and Reiner (2003), which examined the relationship between AEWs and squall lines in west Africa.

Fink and Reiner (2003) tracked both AEWs and squall lines over west Africa to study the potential relationship and interactions between the two events. The authors developed a set of phase definitions for the AEWs based on streamlines and bandpass filtered winds and determined the AEW phase in which the squall line was embedded. For the period studied, May-October 1998 and 1999, they found that 42% of squall lines identified were determined to be forced by AEWs, and 66% associated in some way with AEWs. Of the squall lines associated with AEWs, they found that nearly half of AEW-related squall lines formed west of the wave trough. The AEW-associated squall lines had no distinguishing characteristics from those that were not associated with AEWs, leading the authors to conclude that it is more likely that AEWs mainly play a role in the development of squall lines in west Africa, rather than modulating their characteristics.

In some cases, AEWs may be more closely linked with excessive precipitation in west Africa. Engel et al. (2017) documented two such cases, where slow-moving AEWs generated mesoscale convective systems (MCSs). The authors concluded that these MCSs were distinct from the more typical, faster-moving systems discussed in papers like Fink and Reiner

(2003). Rather, the MCSs were more closely embedded in the cyclonic flow around the AEW, and were observed to have some degree of rotation associated with them. The authors also concluded that the AEWs enhanced the available moisture in the environment, making it possible for the MCSs to produce extreme amounts of rain.

In their paper on types of weather and rainfall over Senegal, Moron et al. (2008) used k-means clustering of the wind field at multiple levels to classify the weather patterns for the surrounding region. Of the eight weather types identified, five were associated with AEWs and monsoon surges, and were found primarily during the summer months. Three of these summertime patterns additionally had anomalously high rainfall over Senegal. However, the authors noted that some of these patterns may be different phases of the AEW's life cycle or propagation, rather than distinct patterns. Increased precipitation was typically associated with southerly wind anomalies over the region, which includes some phases of AEW.

In addition to identifying synoptic-scale activity in the Australian monsoon region, as described in Section 1.1, Berry et al. (2012) also examined the rainfall contributions of the systems they identified to the region. Using a broad spatial and temporal area for association, they estimated that 40-50% of summertime rainfall in regions of Australia equatorward of 20°S was associated with a PV maximum.

Dominguez et al. (2020) also examined the precipitation associated with the TEWs tracked in their study. Across the Atlantic Ocean, the authors contributed 30-50% of the summer rainfall to TEWs. Over Central America and into the eastern Pacific, however, they found the percent contribution to be in excess of 50%. The authors also found that the annual variation in TEW-associated rainfall was correlated with El Nino-Southern Oscillation (ENSO) phase, which they hypothesized is due to the relationship between ENSO and TC development.

1.3 TEW Tracking Methods

Depending on the goals of a study, different methods may be used and combined to identify and track TEWs. While a number of tools exist to track TEWs, or any other desired feature, they can broadly be classified as manual, statistical, and automated (e.g., Fink et al. 2004; Chen 2006).

In small studies and operational settings, TEWs are often manually identified from a combination of surface analyses, satellite images, and streamlines at various altitudes. However, even when analyzing one summer over Africa, Carlson (1969) noted that these manual methods are imperfect, and benefit from knowledge of the wave's full life in order to prevent irregularities. When developing a global climatology of TEWs and studying their activity over an extended period of time, manual analysis and adjustment is not practical, and statistical or automated approaches become necessary.

Rather than analyzing individual tracks, statistical methods, such as power spectral analysis and bandpass filtering, directly return information about the levels of TEW activity (e.g., Dickinson and Molinari 2000; Wheeler and Kiladis 1999). These methods show whether there is power in appropriate variables at the time scales of TEWs for the area they are applied to. Depending on the methods and how results are displayed, this can provide information on the signal strength and significance, spatial structure, and general preferred path of waves. These methods have worked well for AEWs, which are very regular during the boreal summer, but may pose problems in regions where the TEW return period is more variable (Chen 2006; Berry et al. 2012).

Automated objective tracking algorithms generally work by identifying individual waves from a dynamical field. This can be done in a number of ways, which will be described in more detail below. In general, the user supplies data fields and sets a threshold for identifying features, as well as a minimum duration for the feature's lifespan. For TEWs, these types of

trackers often use various flavors of vorticity (e.g., Brammer and Thorncroft 2015; Hurley and Boos 2015; Thorncroft and Hodges 2001). While these types of trackers allow users to analyze large spatial and temporal domains and create extensive TEW climatologies, Thorncroft and Hodges (2001) notes that objective tracking is also limited by the user-defined thresholds. Weak waves that do not meet the tracking threshold, especially when the wave is early in its lifecycle, may not be tracked, potentially biasing the results.

Hovmöller trackers, such as the one employed by Brammer and Thorncroft (2015), work by identifying the time-longitude tracks of TEWs and then reconstructing the latitude-longitude track from it. These trackers first average the data field over a latitudinal band appropriate to the region. These latitudinally averaged fields are then used to create Hovmöller diagrams of time versus longitude. Software can then trace the path of the wave through the Hovmöller diagram to create time-longitude tracks. Using the time-longitude tracks, latitude-longitude tracks can be reconstructed through weighted averages to find the centroid of the area of increased the tracking variable. However, because latitudinal information is compressed in the latitudinal averages, it may be challenging to recreate the wave's track if there are multiple waves at different latitudes, which may happen over North Africa.

Feature trackers identify waves using extrema in the data field and connecting extrema through time (e.g., Hodges 1995; Thorncroft and Hodges 2001; Ullrich and Zarzycki 2017). While multiple trackers of this type exist, they follow a similar set of steps, identifying extrema in the data field, determining if the extrema meets the desired threshold, and connecting the points through time. Because no latitudinal averaging is applied, the resulting tracks do not require additional steps to identify both a latitude and longitude for the wave, and multiple waves can exist at different latitudes of the same longitude. However, most feature trackers only identify individual points. For TEWs, this results in distilling broad trough axes to single points. Therefore, feature trackers assume that the maximum in the tracking field are located along or acceptably close to the trough axis.

The Belanger et al. (2016) tracker is based on feature tracking, but uses additional processing to recreate the entire trough axis rather than an isolated point, allowing it to return additional variables about the wave. Through analysis of the tracking field, as well as additional variables, the authors approximate the entire trough axis and spatial extent. This allows the waves to be associated with other variables, such as precipitable water and outgoing longwave radiation, over broader areas.

Automated trackers are generally more computationally expensive than statistical methods, but return more information about the individual waves. Various post-processing of individual wave tracks also allows greater flexibility in compositing the structure of features around the waves, such as clouds and precipitation.

1.4 Goals

While regional studies are valuable, not all regions have been equally studied, and there is a lack of global perspective on TEW activity and their contributions to precipitation across the tropics. Based on the variety of regions where TEWs have been identified, as discussed in Section 1.1, it seems likely that TEWs can be found throughout the entire tropics, with preferred areas including the North Atlantic and eastern North Pacific Oceans. Using a global domain to track TEWs removes this limitation of regional studies, and may allow us to find additional regions of enhanced TEW activity. Using full years rather than summertime-only domains also allows for an examination of the seasonal cycle of TEW activity. Potential seasonal variations in TEW activity have not been well studied, with the vast majority of studies focusing solely on summertime activity.

In addition to broadening our knowledge of when and where TEWs occur, studying the precipitation associated with them provides context for their contributions to weather across

the tropics. TEWs have been shown in regional studies to contribute up to 50% of summertime rainfall in various regions (e.g. Fink and Reiner 2003; Berry et al. 2012; Dominguez et al. 2020). Therefore, we expect that TEWs compose a significant portion of the total annual rainfall across the tropics, especially in regions with increased TEW activity.

The creation of a global climatology of easterly waves can help to fill these knowledge gaps and serve as a starting point for studying the precipitation of TEWs across the tropics. This may be useful for a number of reasons. Because TEWs are associated with variation in tropical rainfall, including extremes, understanding their variation is important not just for scientific understanding, but may also have practical implications for applications like agriculture and water management. The length of the track climatology may be useful for further studying how TEW activity has changed in response to global climate. Complementing this, the availability of precipitation data for the later half of the track database may be useful in creating additional ways to classify TEWs besides the atmospheric level and region in which they were tracked.

Therefore, our goals are to create a global database of TEW tracks, analyze the characteristics of these tracks, and to associate these TEWs with precipitation to analyze how TEWs contribute to rainfall throughout the tropics. While we expect to find TEWs throughout the tropics, we also expect for there to be preferred regions of activity that support TEW development and propagation, especially where PV gradients exist. Total precipitation associated with TEWs is likely related to both the presence of TEWs and available moisture. While we expect TEWs to be notable contributors to total annual rainfall, we do not expect the summertime values, in the range of 30-50%, to be representative of the fraction of total annual precipitation that can be associated with TEWs.

Chapter 2

Tropical Easterly Wave Activity

2.1 Data and Methods

2.1.1 Data

Because this research was funded under NASA's PMM Science goals, the dynamical fields for tracking came from the Modern-Era Retrospective Analysis for Research and Applications, Version 2 (MERRA-2) (Office and Pawson 2015). MERRA-2 has a spatial resolution of 0.625°x 0.5°, a 3-hourly temporal resolution, and covers a global domain. At the time this project began, the years 1981-2018 were available. While the choice of reanalysis has an impact on the number of TEWs that can be identified by a given method, Belanger et al. (2016) has shown that we should expect similar areas of increased TEW activity regardless of data choice. In addition, the methods outlined below could easily be applied to other reanalyses.

As noted in Section 1.1 northern and southern track AEWs have varying structures, and the structures of TEWs in other regions is less well documented. Therefore, we tracked TEWs globally at both 850 hPa and 700 hPa to increase our ability to identify TEWs regardless of which level their circulation is stronger at. Tracking at both levels also makes it easier to compare our results with existing climatologies, as these are the most commonly used levels in the literature discussed in Sections 1.1 and 1.3.

Before running TRACK, it is important to pick an appropriate data field for identifying TEWs. Older literature on tracking cyclonic features has used relative vorticity (e.g., Thorncroft and Hodges 2001). While relative vorticity is easy to calculate, decomposing it into its natural coordinate components reveals a potential complication. The decomposition of vorticity into its natural coordinates is shown in Equation 2.1, with V as the wind speed, R_s as the radius of the streamline, and n as the vector normal to the streamline.

$$\zeta = -\frac{\delta V}{\delta n} + \frac{V}{R_s} \tag{2.1}$$

In this framework, vorticity is composed of a shear component, the first term in equation 2.1, and a curvature component, the second term in the equation. If we apply this framework to a zonal jet, as shown in 2.1, we see that there is relative vorticity along a jet, even though there is no curvature to the flow, due to the shear on either side of the jet. While shear vorticity alongside a jet may play a role in the intensity of the wave, we expect some curvature in the flow around a TEW. Including shear vorticity may also introduce additional non-waves to a TEW database, or give the impression that the TEW is stronger, as measured by its vorticity.

By using curvature vorticity (CV), we can bypass this concern altogether (e.g. Brammer and Thorncroft 2015; Brannan and Martin 2019). Instead of relying other means to filter out areas of cyclonic relative vorticity dominated by the shear component, using CV lets us focus on features with curved flow. While the curvature term could be calculated directly, calculation of the radius of curvature R_s is complicated and prone to error. Instead, by rearranging Equation 2.1 and expanding the shear term, we can calculate CV using only the u and v components of the wind, as shown in Equation 2.2. Relative vorticity was not decomposed for simplicity's sake, but was calculated from the wind components for consistency.

$$\frac{V}{R_s} = \zeta + (\frac{-v\delta V}{V\delta x} + \frac{u\delta V}{V\delta y}) \tag{2.2}$$

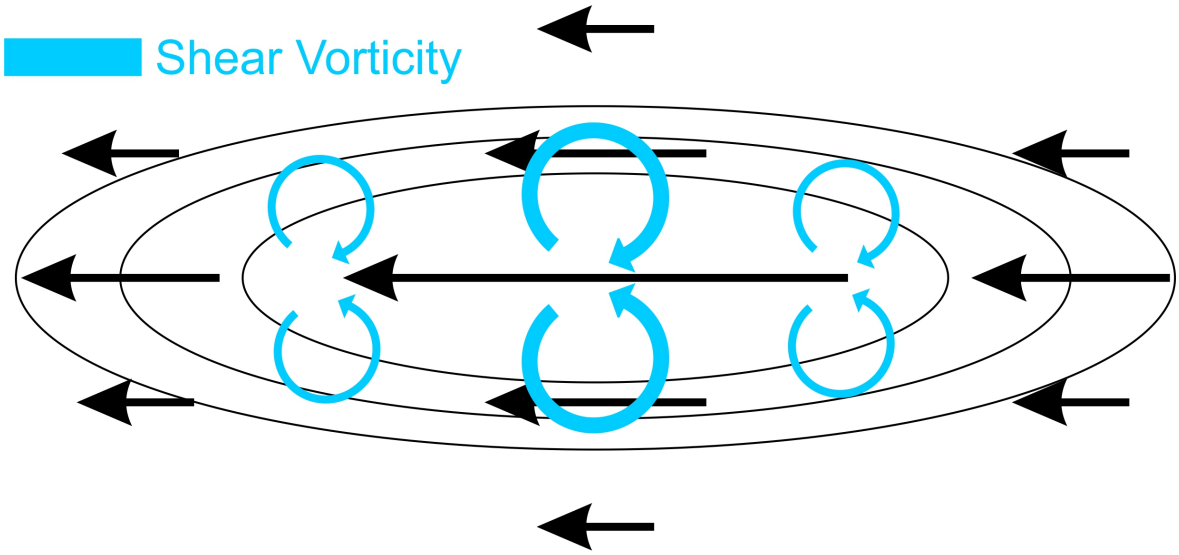

Figure 2.1: An idealized zonal easterly jet. Wind is shown in black arrows, isotachs in black contours. Shear vorticity is annotated in light blue, and curvature vorticity is annotated in purple.

2.1.2 Running TRACK

We chose to use TRACK to identify TEWs because it is well-established in literature for tracking TEWs (e.g. Thorncroft and Hodges 2001; Serra et al. 2010; Hurley and Boos 2015). TRACK is a feature tracker, and has the benefits and limitations outlined in section 1.3. The program and the underlying theory are described in more detail in Hodges (1995) and Thorncroft and Hodges (2001). In addition to the general limitations of feature trackers, TRACK does not discriminate between origin latitude or direction of propagation. The result is initial output that includes every cyclonic feature in the supplied data. Therefore, multiple steps of post-processing after running TRACK are required before analyzing TEWs, which will be described in the next section.

TRACK requires unmasked spatial grids, while MERRA-2 masks fields when the pressure level is below ground. Rather than imposing a harsh barrier where the chosen levels are

underground by filling with a set value, we used bilinear interpolation to fill the masked regions after CV was calculated and before running TRACK. This did not introduce excessive artifacts, as most of the affected locations in the tropics are mountains, and do not cover a broad spatial area.

When running TRACK, we used a CV threshold of $1x10^{-5}$ s^{-1} ($-1x10^{-5}$ s^{-1} for SH) for identifying areas of cyclonic CV. TRACK has a default setting that automatically eliminates tracks with lifespans shorter than two days and travel distances shorter than 10° from the final output.

2.1.3 Post-processing of TRACK Output

For the purposes of filtering the TRACK output down to TEWs, we developed a set of criteria for the tracked features to meet. The first step removes all features that originate in the mid latitudes, poleward of 40°, and requires all remaining tropical features to propagate from east to west for a significant portion of their life. This stage still includes TCs that developed from TEWs. In the second step, TCs were removed by matching TEW tracks to the TCs in the International Best Track Archive for Climate Stewardship (IBTrACS) (Knapp et al. 2018).

For the first step of filtering from the raw TRACK output, we used a combination of criteria regarding the first point in the track and the distance and direction the CV feature traveled. All tracks whose first point was poleward of 40° in its respective hemisphere were discarded. Of the remaining tracks, we looked at the CV feature's motion to determine which features were TEWs and which to discard. To be retained as a TEW, the CV feature needed to have a net westward travel distance in the tropics or subtropics of at least 15°. We broadly defined the tropics and subtropics as latitudes equatorward of 40°. Some short-lived TEWs

may have been removed by this process, but the decision was made to ensure that other non-TEW features were removed. This 15° threshold did not discriminate between TEWs and TCs, so TC motion was counted towards a feature being counted as a TEW.

After the first step was completed, the database contained a total of 38723 tracks. Table 2.1 shows the distribution of tracks per level and hemisphere. This first subset of tracks still includes the TC life phase. In the 700 hPa tracks, shown in Figure 2.2, there are numerous tracks in both hemispheres that extend poleward to latitudes in excess of 50°. Similar results are found at 850 hPa, the plot for which can be found in Appendix A. While these complete tracks may be useful in other research, this project aims to focus on TEWs and precipitation they contribute to while they have the characteristics of a TEW. Because of this focus, we removed the TCs by matching the TEW database against IBTrACS.

Table 2.1: Number of tracks for each hemisphere and level, 1981-2018.

	850 hPa	700 hPa
NH tracks	10135	15327
SH tracks	4312	8949
Total tracks	14447	24276

For a TEW to match to a TC in IBTrACS, we required at least five spatio-temporal matches between the TEW track and the TC in IBTrACS, for reasons that will be outlined below. We defined a spatial match as the TEW point and IBTrACS center position falling within 1000 km, calculated using great circle distance, the equation for which is in equation 2.3, where R_E is the radius of the Earth and lat_1, lat_2, lon_1, and lon_2 are the latitudes and longitudes of the TEW and TC. Time matches were exact at the three-hourly analysis times. These matches did not have to be consecutive, as long as they occurred along the same pairing of tracks. However, all points after the first match were removed, including any

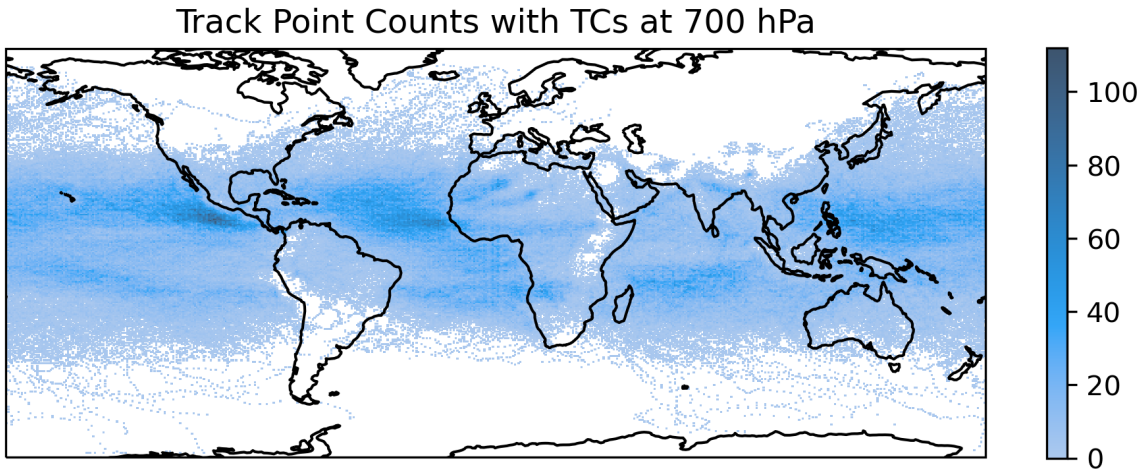

Figure 2.2: Number of TEW track point counts per 0.625°x0.5°grid box, before removing TCs, accumulated over the years 1981-2018, at 700 hPa.

that might be after the TC's dissipation or extratropical transition and not represented in IBTrACS. We chose to give a generous radius for the spatial matches to accommodate both discrepancies that may exist in MERRA-2 as well as biases in TRACK that may displace the identified center of the CV maxima associated with the TEWs. The requirement of five matches times then compensated for the generous radius.

$$dist = R_E * (\arccos(\sin lat_1 * \sin lat_2 + \cos lat_1 * \cos lat_2 * \cos(lon_1 - lon_2))) \tag{2.3}$$

TC removal removed part or all of the track for 2625 and 2627 tracks at 850 and 700 hPa, respectively.

In addition to matching TEWs to TCs, we matched the TEW track points at 850 hPa against those at 700 hPa. Vertically collocating TEW points allows us to identify which TEWs have greater vertical coherence, for the purposes of this project defined as the TEW existing at both 850 and 700 hPa. This distinction will be especially useful when examining the precipitation associated with TEWs in Chapter 3. While vertical collocation does not

entirely illustrate the structure of TEWs, it can provide some insights, as increased cyclonic CV through a vertical column may suggest that the column is more likely to have increased convection and precipitation.

The methods used to vertically match TEW points are similar to those used to match TEWs to TCs, as described above, with some key modifications. Firstly, rather than matching entire track segments, we matched track points. This allows for a pair of TEWs to become vertically collocated and then move out of phase. Second, because these tracks were all generated from MERRA-2 using TRACK, we employed a tighter matching radius of 500 km. Therefore, for TEW points to be vertically collocated, a pair of points at 850 and 700 hPa needed to be at the same time and located within 500 km, as calculated with the great circle distance used before. A 500 km radius is consistent with documented tilts of TEWs (e.g. Schlueter et al. 2019a; Torres et al. 2021). If two points at one level matched to a single point at the other level, only the closest point was retained as the match. A summary of the numbers of points at each level, hemisphere, and matching combination are found in Table 2.2.

Table 2.2: Numbers of TEW points that were and were not vertically collocated, divided by level and hemisphere, 1981-2018.

	850 hPa		700 hPa	
	NH	SH	NH	SH
Vertically Collocated	103244	42597	103244	42597
Not Collocated	246393	124606	392767	270413
Total	349637	167203	496011	313010

2.2 Results

2.2.1 Spatial Patterns

Figure 2.3 shows the counts of track points that fall in each 0.625°x0.5°grid box at 700 (a) and 850 hPa (b), after removing TC tracks. Based on the previous literature discussed in section 1.1, we expect to see strong peaks in TEW activity over west Africa and the tropical Atlantic basin, as well as in the east Pacific, and additional maxima over tropical southern Africa, Australia, and the Indian Ocean (e.g. Hodges et al. 2003; Brammer and Thorncroft 2015; Belanger et al. 2016; Hurley and Boos 2015). The distribution of track points and the areas of increased TEW activity broadly agree with these and other existing climatologies.

While there are clear areas favored for TEW activity, TEWs were tracked across nearly all of the tropics, with few exceptions, particularly mountainous areas, such as the Andes Mountains of South America. The lack of activity near mountains may be explained by the mountains physically blocking the waves from continuing to propagate, or may be a consequence of needing to fill the masked data. From this low-level background activity, the favored latitudes for TEWs, with greater than 40 waves per grid box across the 38 years in this climatology, are within 5° of 15° in both hemispheres. There are many areas of interest both when comparing regions at one level and when comparing the same region at different levels. When looking at the first points in the tracks later in this section, we will expect to see peaks in genesis to the east of the areas with greatest TEW occurrence.

Consistent with papers like Thorncroft and Hodges (2001), which found that northern and southern track AEWs favor developing at 850 and 700 hPa, respectively, there is a difference in the tracks of AEWs when compared between 850 and 700 hPa. Two distinct areas of AEW activity are evident in northern and western Africa, each with 40-60+ waves per grid box compared to the background activity. Southern track AEWs are more apparent at 700 hPa along 10°N as far east as 40°E. Some northern track AEWs are present at 700 hPa, with

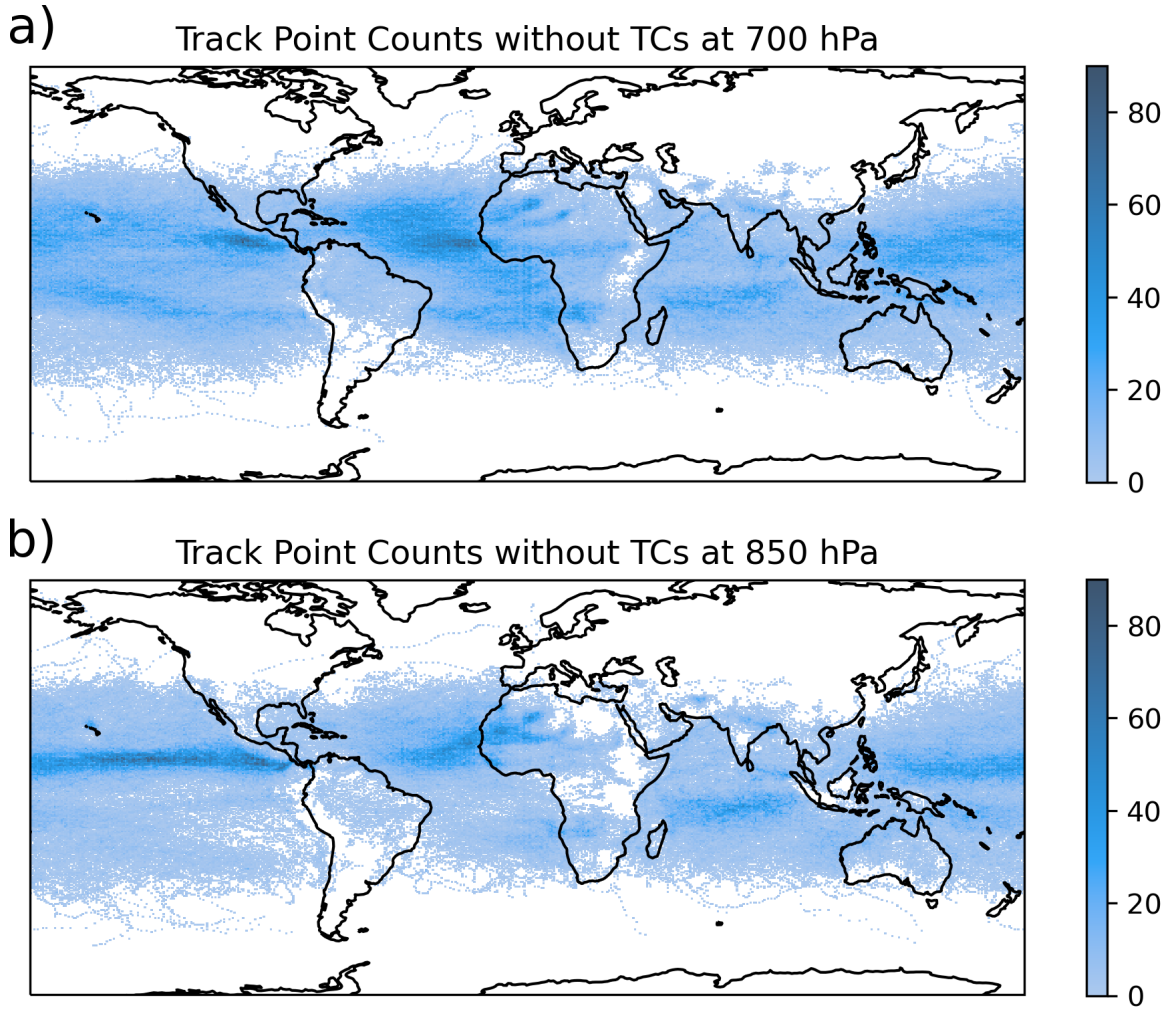

Figure 2.3: Number of TEW track points per 0.625°x0.5° grid box, after removing TCs, accumulated over the years 1981-2018, at a) 700 hPa and b) 850 hPa.

two areas between 0-20°E in the Sahara Desert, but they are clearly more active at 850 hPa, where the area of maximum activity is larger, and peaks with 60-80 waves per grid box. These tracks combine west of Africa, leading to a maximum of 80+ waves per grid box in the area near 20°W, 15°N.

In the east Pacific, the differences in TEW activity come more in the potential patterns of propagation that can be inferred from the track point counts in Figure 2.3. At both levels, the easternmost extent of the local maximum, with 60-80+ waves per grid box, is located near 100°W, 15°N, close to the Central American coast, and extending westward by about 5° of longitude. Looking west from that area, however, the TEW tracks at 700 hPa spread out over a broader area, with the wave counts per grid box decreasing to 40-60 waves per box, when compared with those at 850 hPa, which remain within 5° of the average latitude of the boreal summer ITCZ, along the same 15°N band throughout the tropical North Pacific, creating an associated band where 60-80 waves have been tracked in each grid box.

While these two regions in the NH were expected based on literature like Thorncroft and Hodges (2001), there are additional areas of increased TEW activity at both levels and in both hemispheres that studies like Belanger et al. (2016) and Hurley and Boos (2015) have identified, especially in the SH. At the 850 hPa level, shown in Figure 2.3b, the most notable local maximum in TEW tracks is in the southern Indian Ocean. This area, approximately between 0-25°S and 50-100°E, has a maximum of about 40 waves per grid box range, making it less pronounced than the areas in the North Atlantic and North Pacific, but still an area of increased activity relative to the background activity. Additionally, consistent with Hurley and Boos (2015), which also found an increase in monsoon low-pressure systems over Australia and south of Papua New Guinea, our analysis of TEW activity has 20-40 TEW track points per grid box, a slight increase from the background activity of less than 20 TEW track points per grid box.

The central and eastern south Pacific Ocean, from the coast of South America westwards to 180°W, only has notable TEW activity, with about 40 waves per grid box, at 700 hPa. Closer to the South American coastline, this maximum exists closer to 20°S, with the maximum drifting equatorward further west.

Finally, there is area of increased TEW activity at 700 hPa over and west of southern Africa between 15-20°S, extending from 20°E westward into the south Atlantic Ocean and nearly reaching South America. Much of this yeara has 40-60 TEWs per grid box. This area is accompanied by a smaller area, centered around 15°E, 20°S, at 850 hPa, with 20-40 TEWs per grid box. Given the Kalahari and Namib deserts in this region, as well as the colder waters along the coastline, potential similarities and differences in the dynamics between AEWs in the NH and these SH TEWs is something that needs more investigation.

While the distribution of tracks at each level is useful for inferring patterns, the global nature of this database means that the points at which TEWs are first identified are obscured, making a focus on TEW origin locations necessary. Although a precursor to a wave with CV below the tracking threshold may exist before TRACK identifies it, these first points in the wave tracks will be referred to as genesis points. Figure 2.4 shows the spatial distribution of these points at each level. This figure highlights additional differences between the two levels, especially in the North Pacific Ocean. Figure 2.4b makes it clear that TEWs are generated across the North Pacific Ocean throughout the entire wave track along 15°N, especially at 850 hPa, something that could not have been determined from the track point counts in Figure 2.3b alone.

Comparing the representation of AEW genesis between the two levels, northern track waves favor developing closer to the surface, with Figure 2.4b showing waves at 850 hPa developing along a broad path corresponding with the wave tracks, which begins around 10°E, 25°N and extends to the southwest. Though less prominent, some northern track AEWs were tracked at 700 hPa in the same region, and along the same path. The preference for

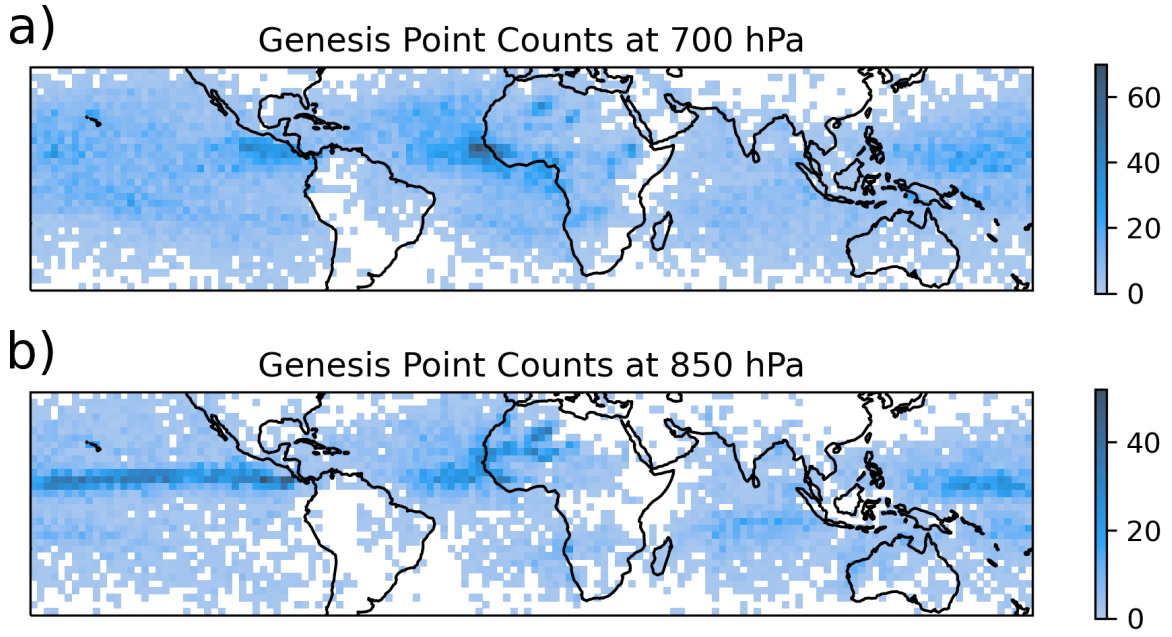

Figure 2.4: Number of first points in TEW tracks per 2.5x2.5 °grid box, after removing TCs, accumulated over the years 1981-2018, for a) 700 hPa and b) 850 hPa.

lower-level AEWs to form further inland is the product of the different dynamical processes that contribute to AEW generation along the northern and southern tracks.

The development of southern track AEWs is most evident at 700 hPa, especially in the Ethiopian highlands, near 40°E, 10°N, and near the Gulf of Guinea, where each of these regions see 40+ TEWs originating in each 2.5x2.5° grid box. Some additional AEWs are generated in the area between these two areas, and westward towards the West African coastline. The most significant region of TEW genesis at 700 hPa in Figure 2.4a is found off of the western coast, near Cabo Verde, where TEWs that originate over Africa emerge over the waters of the tropical Atlantic. This maximum is a key example of the limitations of examining the wave tracks at the two levels separately. It is unclear whether this maximum exists because waves that first developed at 850 hPa deepen in vertical extent her, or if precursor disturbances at 700 hPa intensify as they emerge off of Africa. These precursors may be weak waves, or other features of the weather patterns of western Africa, including

monsoon-related features and MCSs. Studying additional levels and environmental conditions surrounding the wave genesis points may provide some explanations.

Compared to the generation of AEWs and TEWs in the North Pacific, the genesis maxima in other regions are less pronounced, with 20-30 waves per grid box at either level. For the wave maxima in southern Africa around 20°S, both Figure 2.4a and b show most of these TEWs preferring originating over land, near the coastline. Figure 2.4 also shows that TEWs are generated throughout the southern Indian Ocean at 850 hPa.

At the opposite end of the TEW life cycle, Figure 2.5 shows the spatial distribution of the end points of the tracks across the 38 years analyzed. For these figures, it is important to note that track end point is simply the last point in the TEW track. No differentiation was made between whether the TEW dissipated or intensified into a TC. The areas with increased TEW end points are predictably located to the west of the genesis and track point maximums, however their locations relative to those areas has its own interest.

In the eastern North Pacific at 700 hPa, the wave track end point maximum area is at nearly the same place as the wave genesis maximum shown in Figure 2.4, near 100°W, 15°N. Because this short track distance would not have passed through the first round of filtering from the raw TRACK output to TEW tracks, this suggests two main reasons for the increased number of track end points:

1. Waves that develop in the eastern Pacific quickly develop into TCs, and/or waves that have crossed from the Caribbean and Atlantic into the Pacific and are developing into TCs after crossing Central America (e.g. Molinari et al. 2000).

2. The dying waves originated in the Caribbean or Atlantic Ocean, and waves that originate in the eastern North Pacific propagate out into the open Pacific and do not have a preferred termination area.

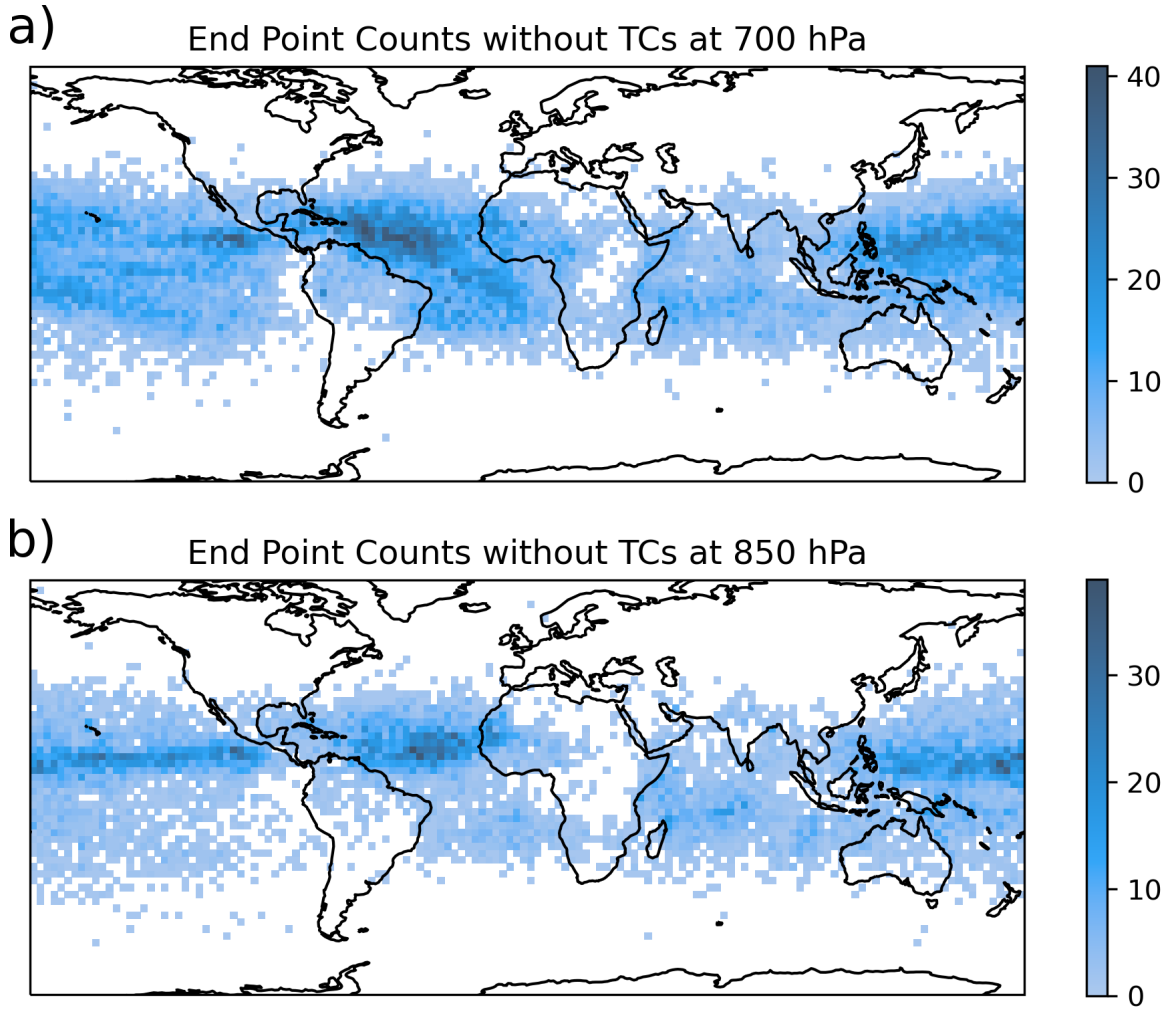

Figure 2.5: Number of last points in TEW tracks per 2.5°x2.5° grid box, after removing TCs, accumulated over the years 1981-2018, for a) 700 hPa and b) 850 hPa.

To determine if one of these reasons explains the peak in end points in future work, or if there is a different cause, the first route of investigation would be the plot the entire track for each wave track that ends in this part of the eastern North Pacific, or even more simply the starting points for these tracks.

In the North Atlantic, the track end locations between the two levels are somewhat displaced, with tracks at 700 hPa tending to terminate further west than those at 850 hPa. Both maxima have broad areas of 40+ wave end points per grid box, but the maxima at 850 hPa is centered near 35°W and the 700 hPa end point maxima is closer to the Caribbean, centered between 50-60°W. While some percentage of these end points come from waves developing into TCs (e.g., Schreck et al. 2011), TCs alone do not seem likely to be the main reason for this westward shift, suggesting differences in wave structures between the two levels.

One way to probe differences in wave structure is through vertical collocation of TEWs. The percentages of wave points that were vertically collocated per grid box are shown in Figure 2.6. Because there are different distributions of TEW tracks at 700 and 850 hPa, both levels are presented as panels a and b, respectively. With little exception, most of the collocated points are located entirely between 40°S and 40°N, despite the fact that the only restriction to these latitudes was for the first point in the track. When a TEW track bends poleward, it becomes an outlier, and its track is often the only one in its grid box, reinforcing that recurving tracks are the exception to the general behavior of TEWs, after TCs have been removed.

Because collocated waves are, unsurprisingly, more common in the previously discussed regions of increased wave activity, it is notable that some key activity regions do not have strong vertical collocation. For example, southern track AEWs, which are found over Africa along 10°N, and found more frequently at 700 hPa, do not have a high rate of vertical collocation, only 10-20%. Those southern track AEWs that were tracked at 850 hPa, however, have a higher rate of vertical collocation, in the range of 40-60%. In contrast, northern

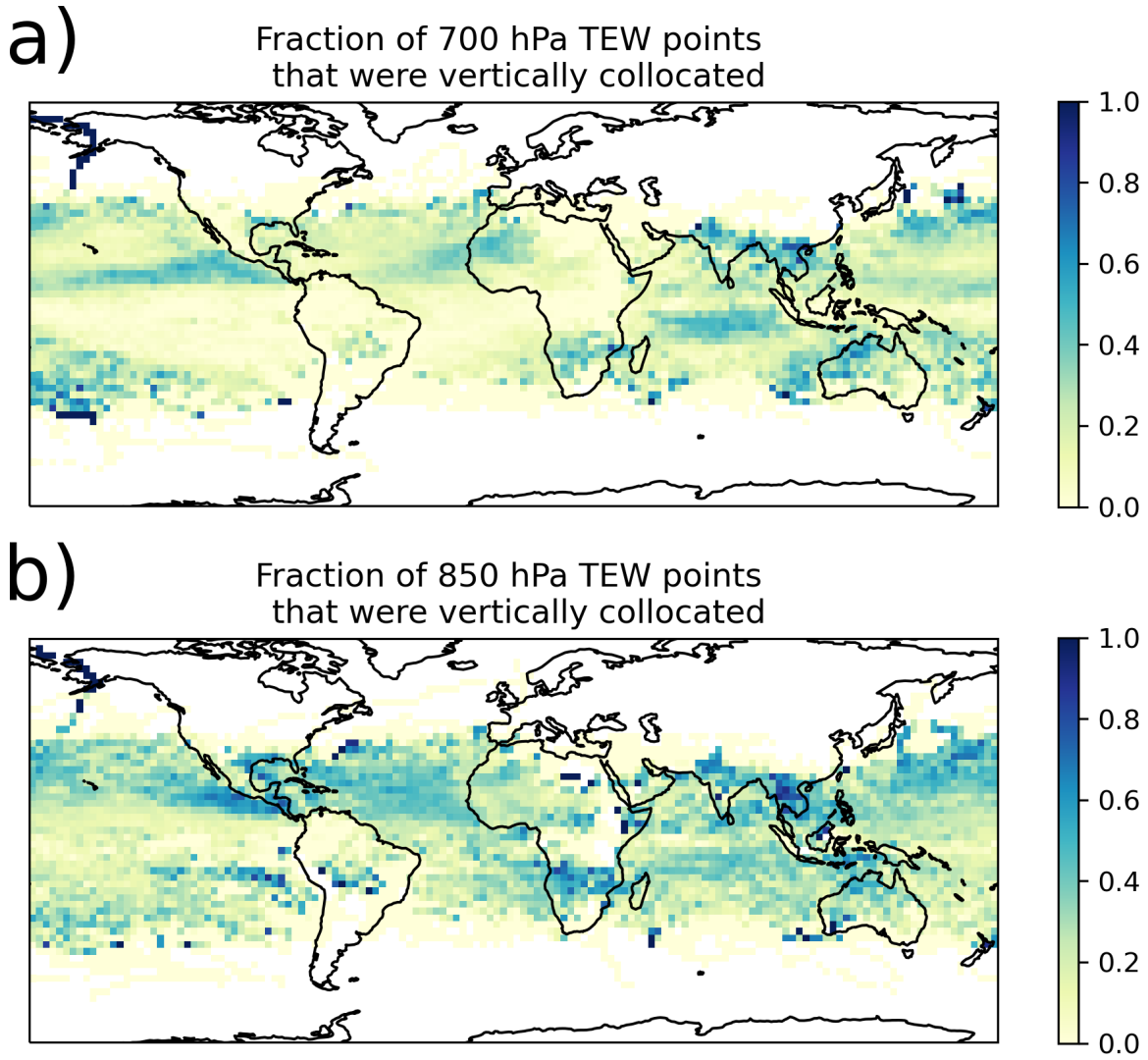

Figure 2.6: Percent of track points per 2.5°x2.5° grid box, after removing TCs, that were vertically collocated, for a) 700 hPa and b) 850 hPa.

track AEWs, especially those that occur further north and east between 20-30°N and near 0° longitude at either level, have comparatively higher matching rates, approximately 50%, regardless of level tracked.

Just as interesting as the regions where TEW points were collocated are the places in the tropics without any vertically collocated points. Complementary to the percentages shown above, Figure 2.7 shows the numbers of track points that were collcoated per grid box. Because the 500 km matching radius is larger then the 2.5° grid box, both levels are shown. Some of regions without any vertically collocated TEW points, such as along the Andes Mountains of South America, make geographical sense. In this case, the mountains may act as a physical barrier for any waves propagating westward from the Atlantic, and new waves may not reach the CV threshold for TRACK until further downstream of the mountains. Equatorial Africa, however, which also lacks vertically collocated TEW points, does not have extreme terrain along the length the equator. While the mountains in eastern equatorial Africa, explain the lack of TEWs along 35°E, the lack of TEWs along the equator stands out, especially in contrast with vertically collocated AEWs to the northwest and the SH African TEW maxima to the south.

2.2.2 Temporal Variability

As an alternate to the aggregate counts that were shown in Table 2.1, Figure 2.8 shows the numbers of waves per year for 700 and 850 hPa. On average, we identified and tracked 380 waves per year at 850 hPa and 638 waves per year at 700 hPa, with standard deviations of 33 and 57 for 850 and 700 hPa, respectively. Because at both levels the average NH wave count is approximately double the SH wave count, the global wave count trend largely mirrors the NH wave count. The SH wave count, however, can magnify a peak or dip, such as the relative drop in the global wave count for 2004. While both years were near average for their wave

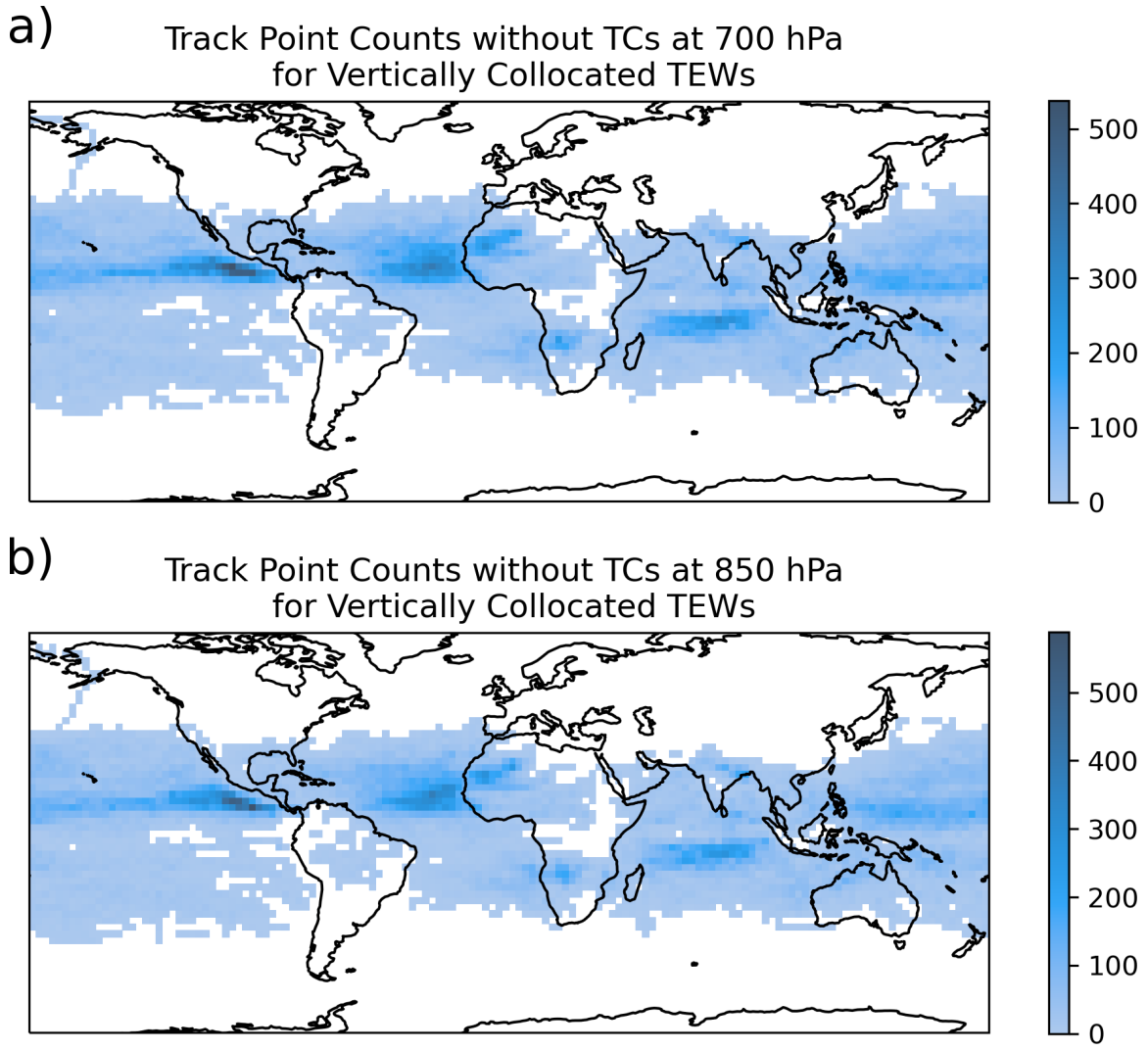

Figure 2.7: Number of vertically collocated points per 2.5°x2.5° grid box, after removing TCs, accumulated over the years 1981-2018, for a) 700 hPa and b) 850 hPa.

counts, the relative peaks in the surrounding years at both levels magnify both the peaks and return to average in 2004.

At the global scale, the correlation between the numbers of TEWs per year for 850 and 700 hPa is 0.639, and this correlation is significant at the 99% level. Due to the larger number of waves, this correlation coefficient is heavily weighted by the NH, which on average has approximately double the number of waves as the SH. For the NH, the correlation between the number of TEWs at each level is 0.685, and for the SH it is 0.436. Both of these correlations are also significant at the 99% level. The reduced correlation in the SH may be due in part to the fact that calendar years were used for this time series, which splits the summer months. Another potential explanation could come from differences in wave structure. With 5-7% fewer points vertically collocated in the SH, this suggests different vertical wave structures between waves at 850 hPa and 700 hPa.

In addition to the similar behavior between the two levels, there is also some shared patterns between the hemispheres at each level. At the 850 hPa level, annual TEW counts in the northern and southern hemispheres have a correlation of 0.502, and at 700 hPa the correlation between the hemispheres is 0.643. Both of these correlations are significant at the 99% level. While the causes for this variability are beyond the intended scope of this research, the presence of prominent peaks and dips in TEW activity suggest that there may be some relation in TEW activity to other phenomena like ENSO. Dominguez et al. (2020) demonstrated that ENSO phase affects the number of TEWs that reach northern South America, and that this in turn affects the precipitation observed in that region. Though further work is needed to test for a relationship, ENSO phase and the resulting anomalies in both atmospheric and oceanic conditions may make some regions more or less conductive to TEW development.

Despite the variability in annual wave counts, there is less variability in the fraction of waves that match to TCs per year. The fraction of TEWs that matched to TCs in each ear are

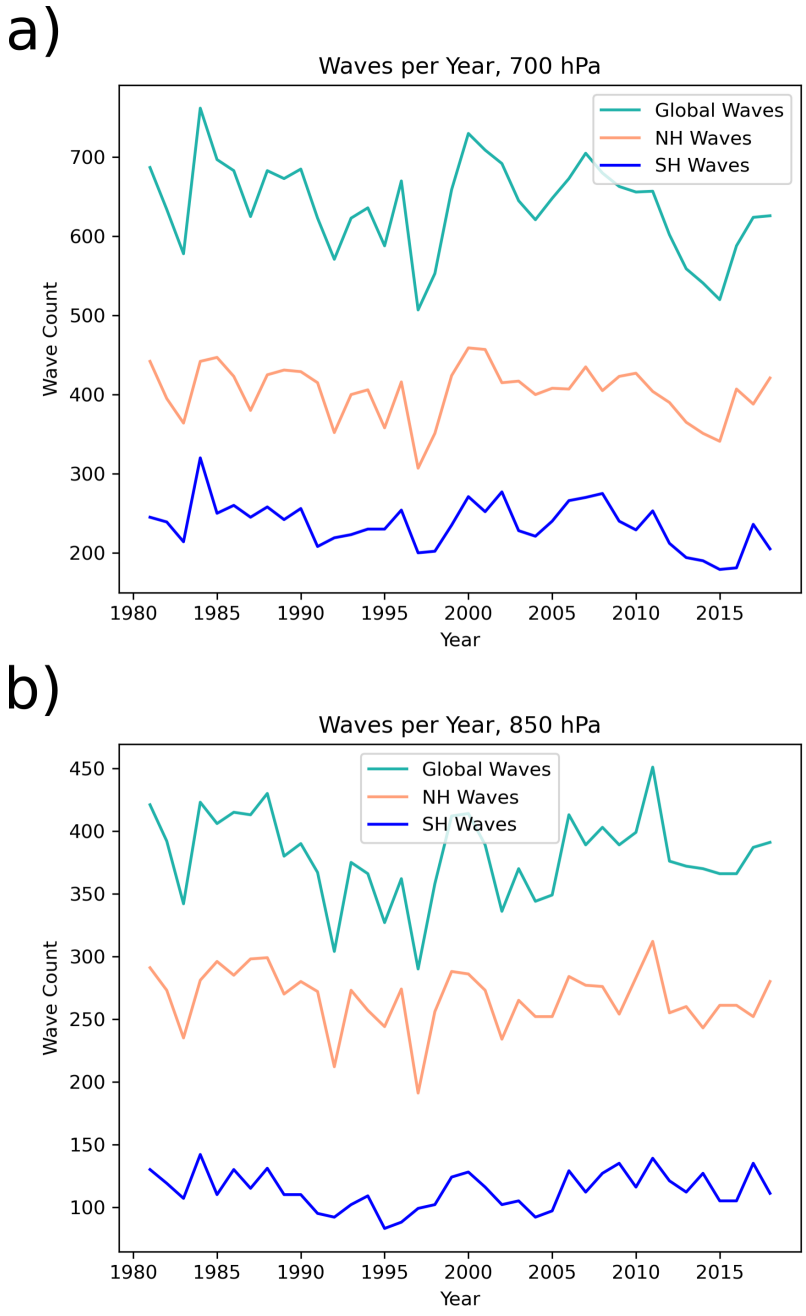

Figure 2.8: Time series of TEWs identified per year for the entire world (green), NH (orange), and SH (blue) at a) 700 hPa and b) 850 hPa.

shown in Figure 2.9. While a the percent of TEWs matching to TCs is higher at 850 hPa, ranging from 10% to nearly 30%, compared to 700 hPa, where 4% to 18% of TEWs match to TCs, because the same number of TCs matched across the 38 years represented, this is almost certainly due to the smaller number of waves identified at 850 hPa than at 700 hPa. Interestingly, at 850 hPa, while typically a smaller fraction of SH TEWs matched to TCs each year when compared to the fraction of NH TEWs matching to TC, there are three cases where a higher fraction of SH TEW tracks matched, 1989, 1996, and 2003.

The numbers of TEWs matching to TCs is well correlated between 850 and 700 hPa, with a correlation of 0.75 significant at the 99% level. The correlations between the matches for each hemisphere are similar, and statistically significant at the same level. Given that the numbers of waves per year are well correlated between the two levels and that the same number of TCs were removed from both levels, this is expected. At either 850 or 700 hPa, the two hemispheres are not strongly correlated, and there is little statistical significance to those correlations.

To complement the time series above in Figure 2.8, Figure 2.10 show the distributions of TEWs per year and season globally and for each hemisphere at 700 and 850 hPa, respectively. The difference in the x-axis scales reinforces the difference in how many waves occur at each level. While on average there are approximately 400 TEWs per year tracked at 850 hPa, the average annual wave count at 700 hPa is approximately 650 TEWs. The quantity of TEWs in the NH compared to the SH means that the annual seasonal cycle of wave counts reflects the cycle in the NH, rather than showing a peak in both JJA and DJF.

Both hemispheres exhibit seasonal cycles in TEW activity, with increased activity in the hemisphere's respective summer and fall months. For both hemispheres at 850 hPa, the average number of waves per summer is approximately double the waves identified in winter. In the NH at 850 hPa, this is an increase from 50 waves per DJF to over 100 waves per JJA

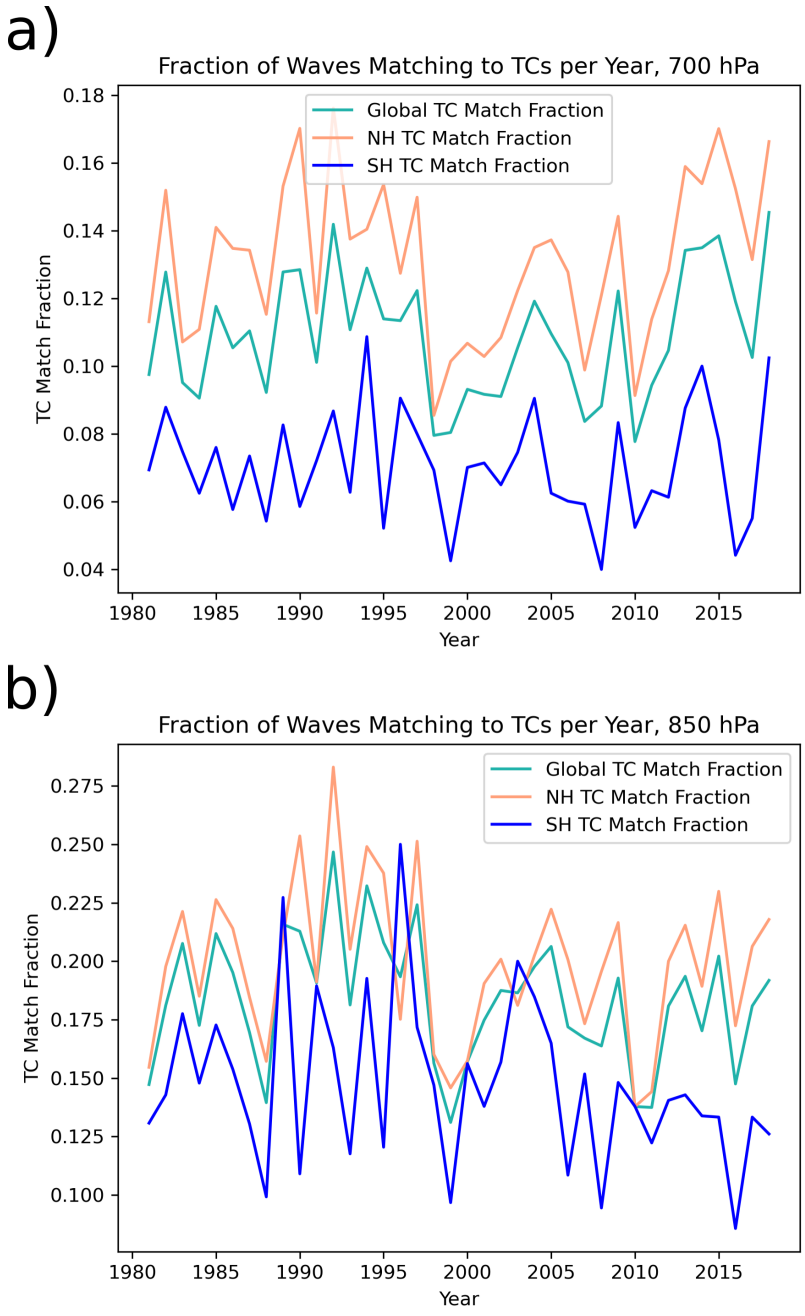

Figure 2.9: Time series of TEWs matching to TCs at 700 hPa for the entire world (green), NH (orange), and SH (blue) for the a) 700 hPa and b) 850 hPa.

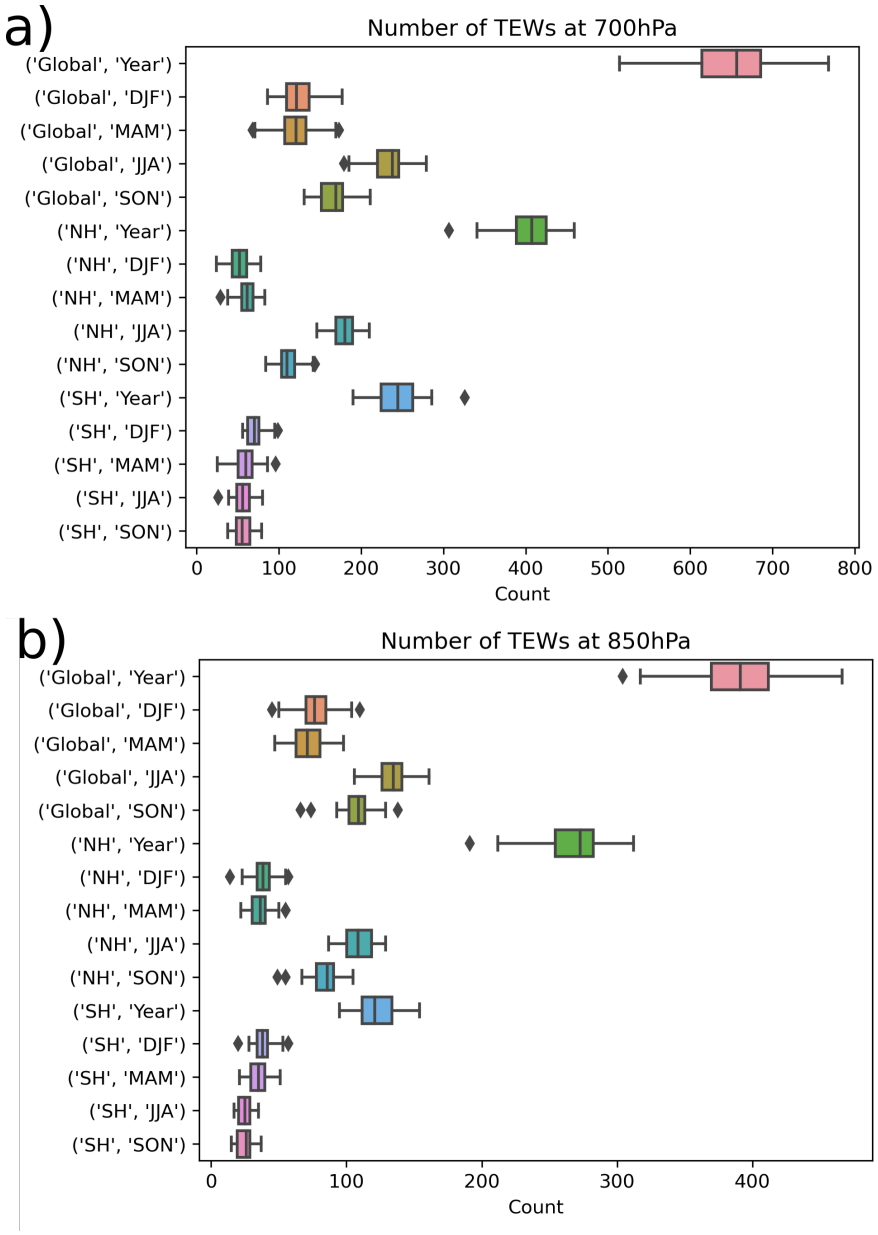

Figure 2.10: Boxplots showing the distributions of waves per year and season globally (top third), in the NH (middle third), and in the SH (bottom third) for a) 700 hPa and b) 850 hPa.

. In the SH at 850 hPa average wave count increases from approximately 25 waves per JJA and SON to around 50 waves per DJF and MAM.

At 700 hPa, the summertime increase is even more pronounced in the NH, where wave counts increase from the DJF average of 50 waves to nearly 200 waves per JJA. This large increase in activity is not present in the SH, where TEW activity increases from an average of 50 waves per JJA to only about 75 waves per DJF. As before, these SH values came from calendar years. Changing the months used for each season, using monthly values, or otherwise accounting for this may change these values slightly, but not enough to change the results.

2.2.3 Wave Characteristics

One of the most obvious ways to verify the importance of removing TCs from the TEW database is through the distribution of TEW maximum intensity, as measured using CV. Shown in Figure 2.11, the TEW maximum intensity distribution is primarily affected at the upper extremes. SH values have been multiplied by a factor of -1 to allow for easy comparison. The median maximum intensity for TEWs at both levels, approximately $2.5\text{x}10^{-5}$ s^{-1}, is not greatly changed. However, at both levels, removing TCs creates a maximum intensity distribution that has fewer and less extreme outliers, and subsequently narrows the interquartile range of the intensities. This narrowing is especially evident at 850 hPa, where removing TCs brings the 75% threshold below $5\text{x}10^{-5}$ s^{-1}.

For the remainder of the results sections, the TEW characteristics discussed were derived from the the tracks that remained after TC removal. As shown above, TC inclusion may introduce biases in the distributions of the variables analyzed.

Without TCs present, the distributions of TEW maximum intensities are similar between the hemispheres and levels. Shown the interiors of each distribution in Figure 2.12, the median maximum CV intensity at both the 850 and 700 hPa levels, regardless of hemisphere,

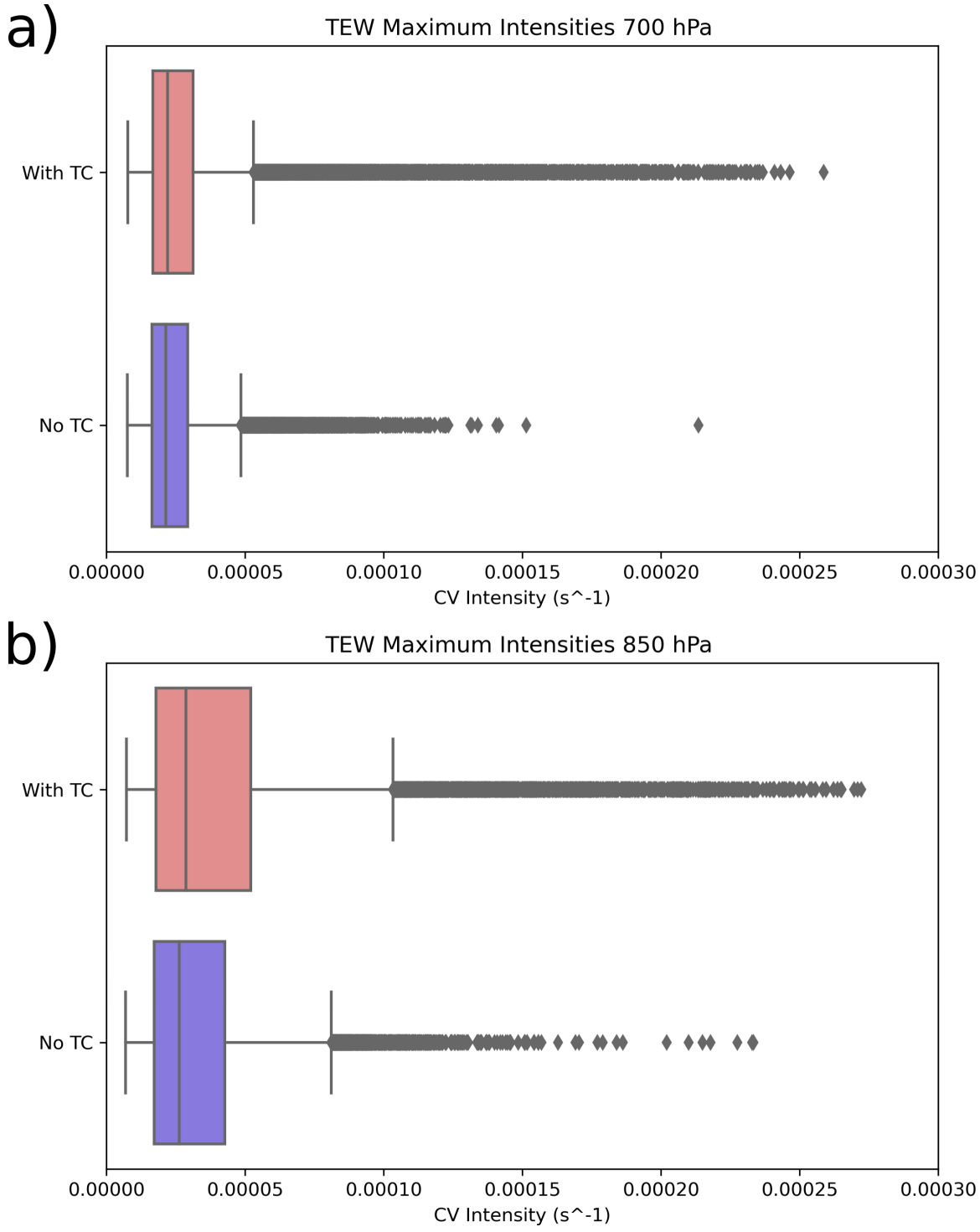

Figure 2.11: Boxplots showing the distribution of TEW maximum intensities as measured by CV (s^{-1}) for the TEW database with (top) and without (bottom) TCs included at a) 700 hPa and b) 850 hPa.

marked with a white dot, is around 2.5x10^{-5} s^{-1}. At both levels, the median for the NH is slightly greater than that for the SH.

For both hemispheres, the distribution of intensities is broader at 850 hPa. The right tail of the distribution narrows closer to 1.0x10^{-4} s^{-1} at 850 hPa, compared to at 5x10^{-5} s^{-1} at 700 hPa. On the left side of the distributions, the secondary peaks may be a result of TC removal, especially as these secondary peaks are stronger in the NH.

The most extreme upper outliers at both levels have maximum CV values between 2.0x10^{-4} and 2.5x10^{-4} s^{-1}. The more extreme intensity outliers are found at 850 hPa. In contrast, the NH at 700 hPa has no anomalous strong TEWs with a CV intensity in excess of 1.5x10^{-4} s^{-1}.

Despite the differences in numbers of waves per hemisphere and per level, TEWs propagation distances are very similar between both the two levels analyzed and between the NH and SH. Shown in Figures 2.13, the majority of TEW track lengths, after removing TC portions of tracks fall between 2000-4000 km, with an average track length of around 3000 km for all levels and hemispheres. These track distances were calculated as the sum of the distances between each point along the track in any direction. Because TCs have been removed from this data, some of the wave distances are shorter than the original 15° threshold used to identify TEWs from the raw TRACK output. These shorter waves tracks were retained because the TC phase was part of that TEW's life.

Across all of our TEW tracks, the average speed for the TEWs we have identified using TRACK in MERRA-2 is 7.5-8 m/s, depending on the level. While there is a broad range of speeds shown in Figure 2.14, ranging from nearly stationary to average speeds in excess of 20 m/s, the majority of waves have average speeds between 5 and 10 m/s. These distributions are also the most symmetric of the wave characteristics shown, suggesting that they are less affected by whether or not a TEW develops into a TC.

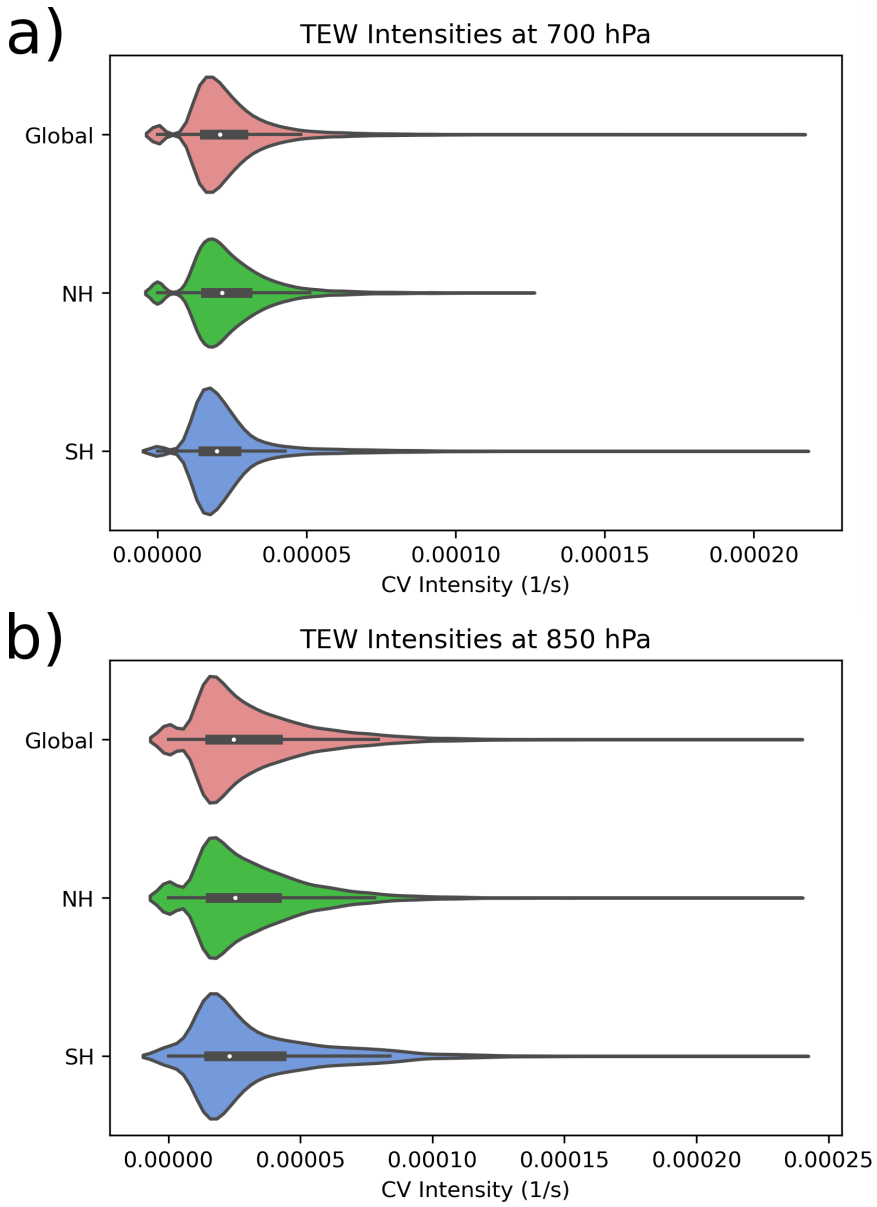

Figure 2.12: Violin plots showing the distribution of TEW maximum intensities, as measured by CV (s^{-1}), globally (top), in the NH (middle), and in the SH (bottom) for TEWs tracked at a) 700 hPa and b) 850 hPa.

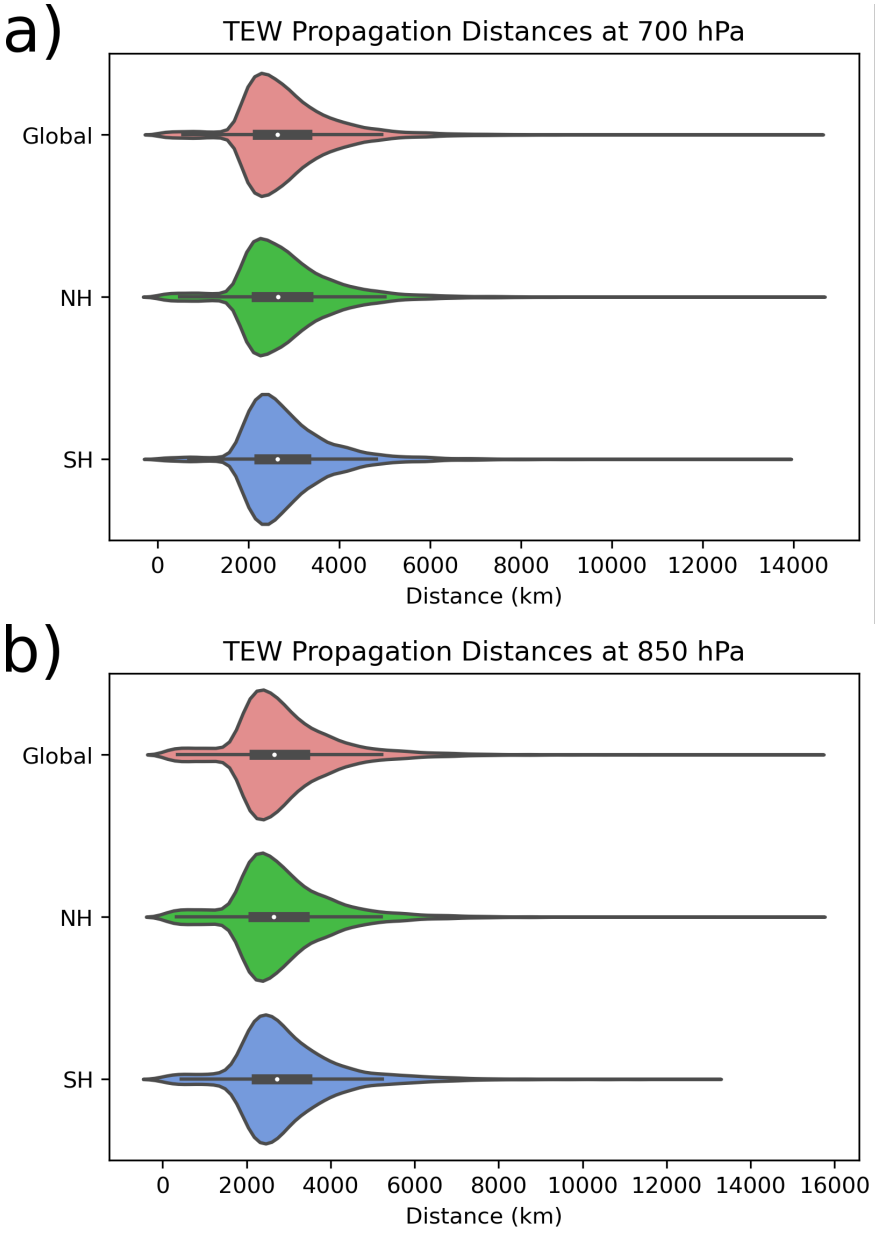

Figure 2.13: Violin plots showing the distribution of TEW propagation distances (km) globally (top), in the NH (middle), and in the SH (bottom) for TEWs tracked at a) 700 hPa and b) 850 hPa.

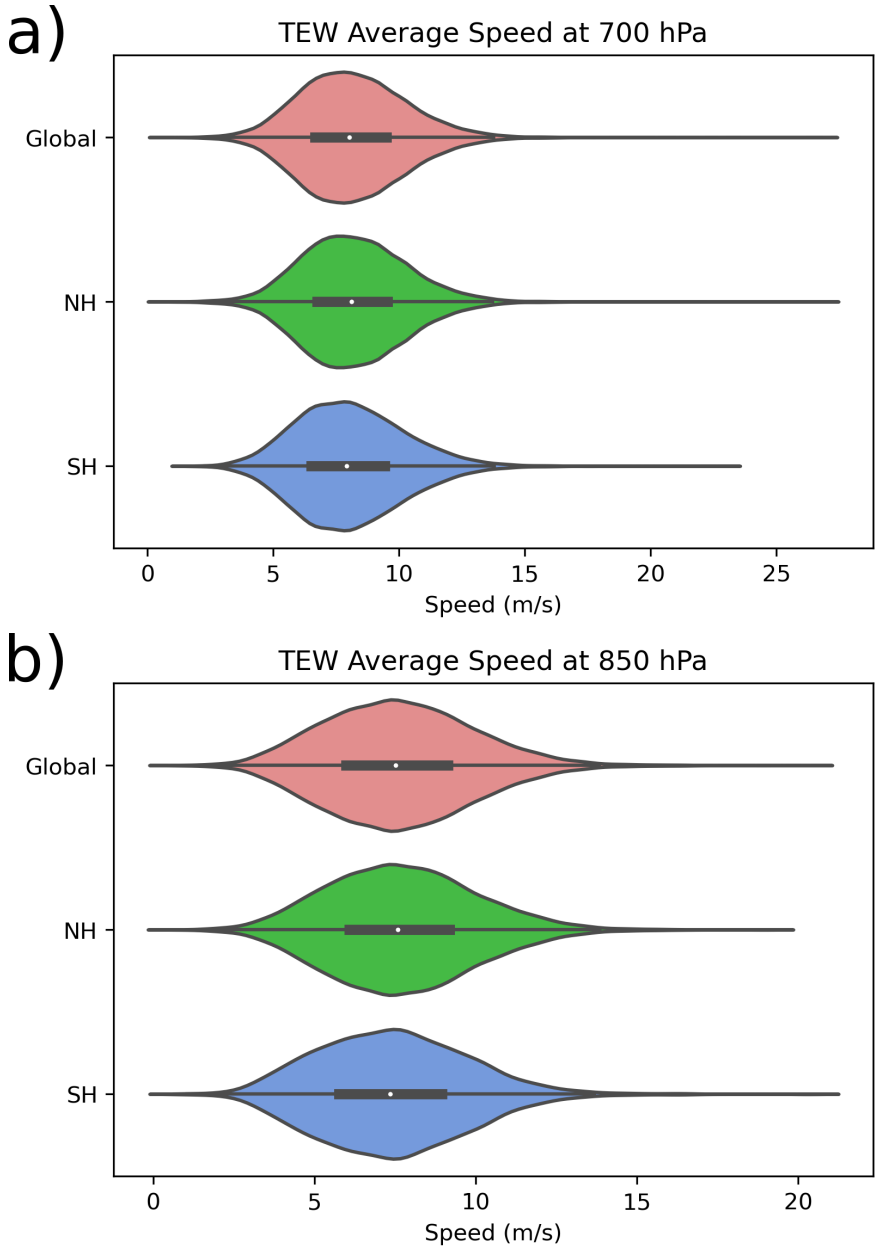

Figure 2.14: Violin plots showing the distribution of the average speeds (m/s) of TEWs globally (top), in the NH (middle), and in the SH (bottom) for TEWs tracked at a) 700 hPa and b) 850 hPa.

This average speed is in agreement with previous literature covering a variety of regions (e.g. Carlson 1969; Fuller and Stensrud 2000; Fukutomi 2019). Propagation speeds are valuable for confirming that these waves are TEWs and not other equatorial waves. The upper bounds of both the 75th percentile and outliers in average speed are more extreme at 700 hPa, which makes physical sense, as winds are typically faster at higher levels of the atmosphere due to lack of friction.

The similarities of the distributions of these wave characteristics points to the overall dynamical similarity of the TEWs identified. While there is likely regional and seasonal variation, on average, our methods have identified synoptic-scale features that propagate from east to west at speeds characteristic of TEWs. With similar distributions of these characteristics in both hemispheres, this supports the conclusion that TEWs are found in the tropical latitudes of both hemispheres. Further investigation of differences in regional and seasonal variation in these variables may be of interest, and may provide insight into potential reasons for variation in these distributions.

Chapter 3

Wave-associated Precipitation

3.1 Data and Methods

To assess the contributions of TEWs to tropical precipitation, we combined the TEW track database described in Section 2 with NASA's Integrated Multi-satellitE Retrievals for GPM (IMERG) calibrated precipitation field, final run, as our precipitation data (GSFC 2019). The final run IMERG calibrated precipitation combines observations from the GPM constellation of satellites with ground-based gauges. While there are other IMERG products available, we will only be using the calibrated precipitation field for this study, and will simply refer to this field as IMERG. IMERG has a native spatial resolution of 0.1°x0.1° covering latitudes from 60°S to 60°N, and native temporal resolution of 30 minutes. IMERG also utilizes reprocessed data from the Tropical Rainfall Measurement Mission (TRMM), and is available beginning June 2000, with new data processed regularly.

To simplify matching with the TEW tracks, the 30-minute IMERG rain rates were averaged to create 3-hourly average rain rates centered on the same analysis times as the TEW track times. To keep comparisons between full calendar years, we decided to only analyze precipitation from 2001 to 2018, the end of the TEW database, rather than including June-December 2000. In total, between both levels analyzed and both hemispheres, this eighteen-year period includes 18,269 TEW tracks composed of 624,019 track points. For the period considered here, 3.1 shows how these points were distributed across the levels and hemispheres. For each level and hemisphere combination, the percent of points that

were vertically collocated only varies from the full period of record for TEW tracks by approximately 1%. Therefore, we will consider the 2001-2018 subset of TEW tracks as being representative of the broader TEW track database.

Table 3.1: Numbers of TEW points that were and were not vertically collocated, after TC removal, divided by level and hemisphere, 2001-2018.

	850 hPa		700 hPa	
	NH	SH	NH	SH
Vertically Collocated	47175	19874	47175	19874
Not Collocated	118832	61358	187744	121987
Total	166007	81232	234919	141861

While TEWs vary in size, we chose to use a fixed radius of 500 km, with the CV center identified by TRACK as the origin, to associate rain with the influence of a TEW. This radius encompasses most of the convective area surrounding a TEW, without being excessively contaminated by other rainfall that is not associated with the TEW, and has been used in similar studies on TC, such as Jiang and Zipser (2010). Similarly to the matching described in Section 2.1.3, we used great circle distance, Equation 2.3, to determine the distance from the vorticity center. The fixed radii of this scale, in degrees or kilometers, have been used in numerous studies on both TEWs and TCs as a way to associate and attribute rainfall to a features (e.g. Jiang and Zipser 2010; Dominguez et al. 2020).

Because this method only identifies rain near a TEW and does not consider other factors that contribute to the formation of convection and precipitation, we cannot say that the TEWs directly cause of rainfall in their vicinity. Rather, the TEWs are associated with the rainfall and may modulate their environments leading to increased rainfall. Potential interactions affecting variability in TEW precipitation are discussed in Section 4.2.

3.2 Results

3.2.1 Global Patterns

The total precipitation associated with TEWs globally across the 18 years analyzed exceeded 5000 mm in select locations, most notably across the tropical North Pacific Ocean for TEWs tracked at 850 hPa. Unsurprisingly, the total precipitation associated with TEWs, shown in Figure 3.1, is largely coincident with the areas of maximum TEW activity discussed in Section 2.2.1. Not all areas of increased TEW tracks have associated rainfall maxima, however. Despite notable TEW track activity, there is little rainfall from TEWs identified over the Sahara desert, a logical result given the lack of moisture.

In 3.1, the accumulated rainfall at any given point is the result of the number of TEWs that occur near it and the amount of precipitation associated with TEWs, which may vary with TEW life stages. In some cases, the TEW-associated precipitation maximum covers a wider area than the wave track maximum, such as in the Bay of Bengal, where a small increase in TEW tracks generates a more perceptible increase in accumulated associated rainfall. In the Bay of Bengal, this creates an area where the total TEW-associated rainfall exceeds 2500 mm, with pockets that exceed 5000 mm. Similarly, while the broad area of increased TEW activity over southern Africa is only modestly more active than the background activity, the waves in this area are associated with 1000-2500 mm of rain, which is comparable to the precipitation associated with southern track AEWs. More work is needed to determine reasons for this, as well as differences between these TEWs and southern track AEWs in the NH.

Annually averaged, however, TEW-associated rain, regardless of the level the TEWs were tracked at, rarely exceeds 500 mm, as shown in Figure 3.2. Similar to the areas of increased total precipitation, the areas of increased maximum precipitation are mainly over tropical oceans where TEW track maxima were found, such as the North Atlantic Ocean in

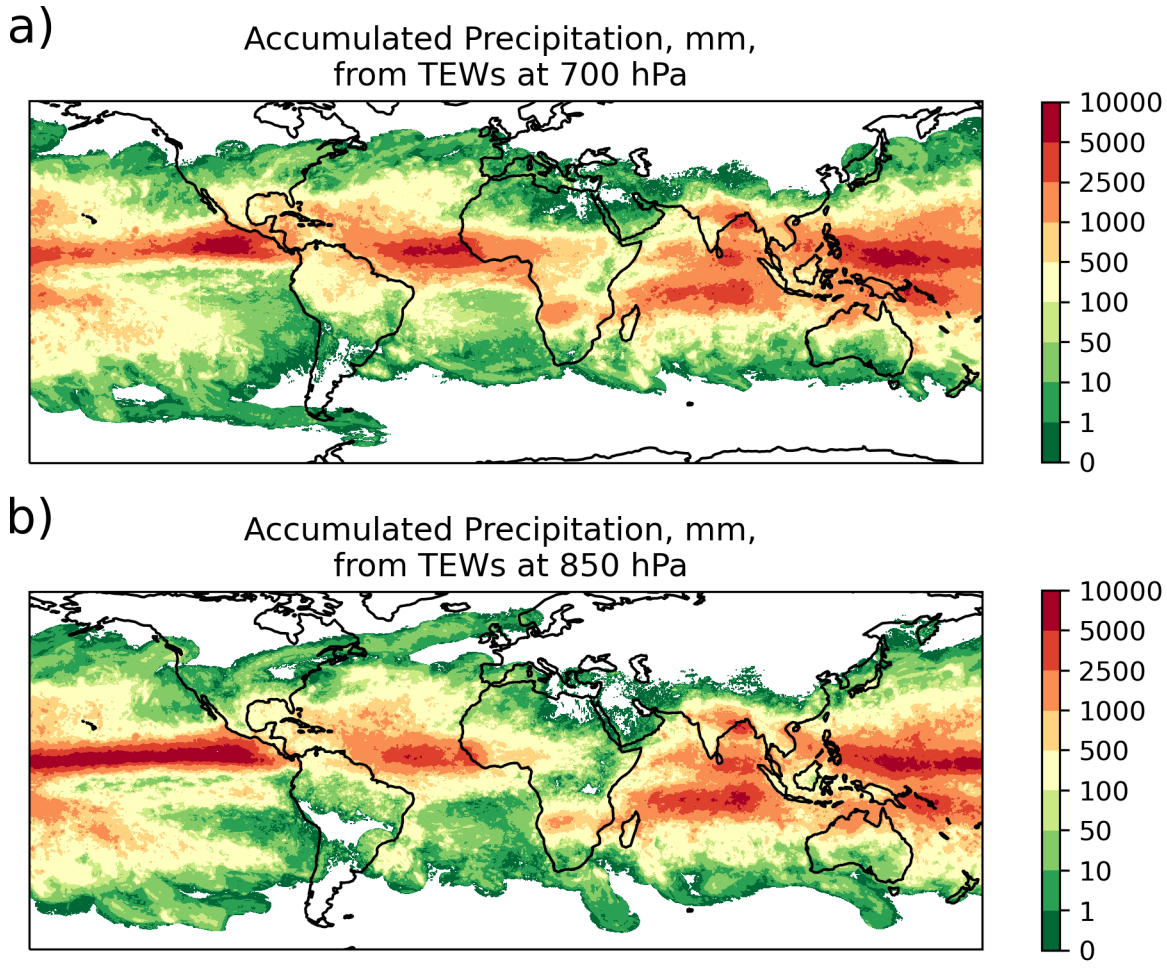

Figure 3.1: Total accumulated precipitation (mm) associated with TEWs tracked at a) 700 hPa and b) 850 hPa, for 2001-2018.

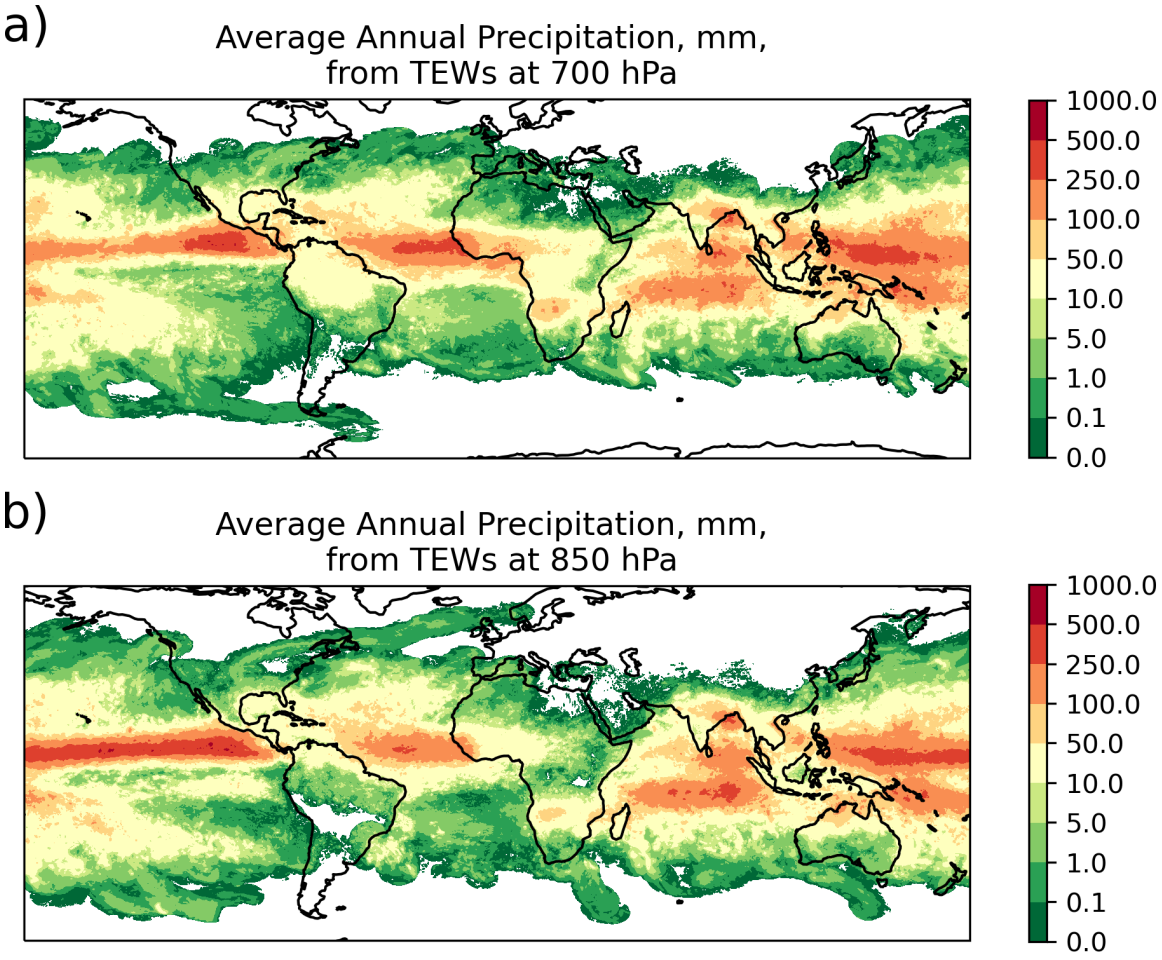

Figure 3.2: Annual average precipitation (mm) associated with TEWs tracked at a) 700 hPa and b) 850 hPa for 2001-2018.

the band centered near 10°N, the tropical North Pacific along 10-15°N, and in the southern Indian Ocean near 10°S.

While the annual average rainfall associated with TEWs varies across the tropics, from less than 10 mm in places including the Sahara, parts of India, and northern Brazil, depending on which level of TEW tracks is considered, the fraction of the total annual precipitation that TEW contribute to is more uniform, with TEWs tracked at 850 hPa contributing 1-5% of the

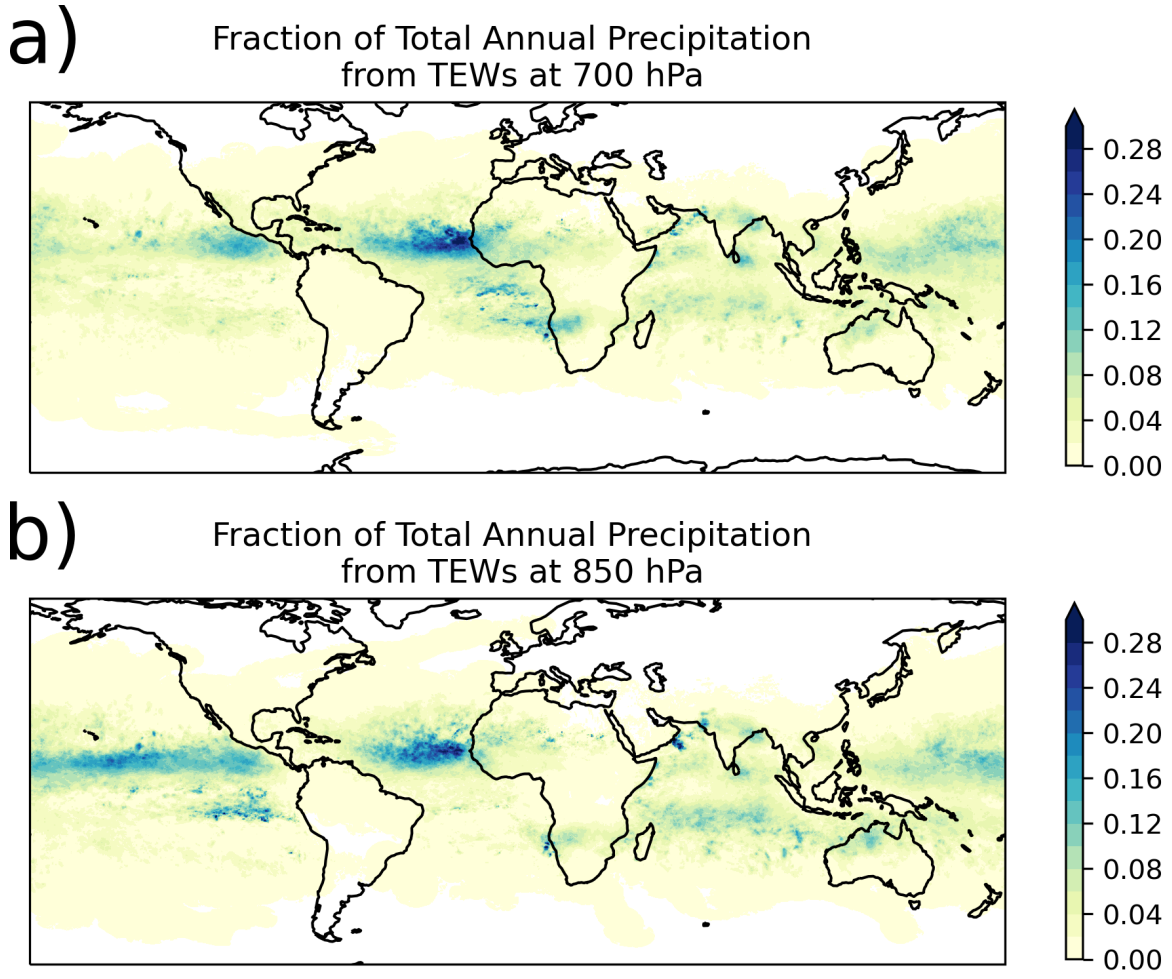

Figure 3.3: Average fraction of total annual precipitation associated with TEWs tracked at a) 700 hPa and b) 850 hPa for 2001-2017

total annual precipitation across most of the tropics. The percent contributions from TEW-associated rain go up to approximately 25% in regions with higher occurrence of TEWs, such as the tropical North Atlantic Ocean. Shown in Figure 3.3, TEWs are rarely associated with more than 30% of the total annual rainfall at any given point.

The fraction of total annual precipitation puts TEW precipitation in the context of the region's typical rainfall. For example, while northern track AEWs have less total rainfall associated with them, they are associated with similar percentages of the annual rainfall to

southern track AEWs, between 10 and 15% of the total annual precipitation. Other regions over land, including southern Africa and northern Australia, also see similar percentages of rainfall associated with TEWs.

While it is less surprising that TEWs in the northern Atlantic and Pacific are associated with more than 20% of the total annual rainfall along the preferred wave tracks, these percent contributions also yield the interesting observation that TEWs tracked at 850 hPa in the southern Pacific Ocean along 5-10°S and between 80-120°W contribute to 20-30% of the total annual precipitation. This is especially surprising because these waters are typically colder, and, as seen in 2.3b, there was no major increase in TEW counts in this region from the background wave activity.

TEWs identified at 700 hPa in the southern parts of Africa and in the south Atlantic Ocean were also associated with 10-15% of the total annual rainfall. While AEWs still contribute more total rainfall and a greater fraction of the total annual rainfall in western Africa, the contributions from these and other SH TEWs should not be ignored.

The total precipitation associated with TEW points that were and were not vertically collocated are shown in 3.4 and 3.5, respectively. As with the locations of collocated points, the precipitation associated with vertically collocated TEWs is constrained to latitudes equatorward of 40°.

In Figure 3.4, the areas that stand out the most are the areas near the equator without any TEW-associated precipitation over Africa, the equatorial eastern Pacific, and much of South America. Most notably, there is a complete lack of TEW-associated precipitation from vertically collocated TEWs over much of South America. Unlike equatorial Africa, where there are also no vertically collocated TEW points, Figure 2.6 shows that there are some vertically collocated TEW points over South America.

In the western parts of the North Atlantic, extending into the Caribbean Sea, Figure 3.5 features a broader area of increased precipitation, between 500 and 1000 mm in total,

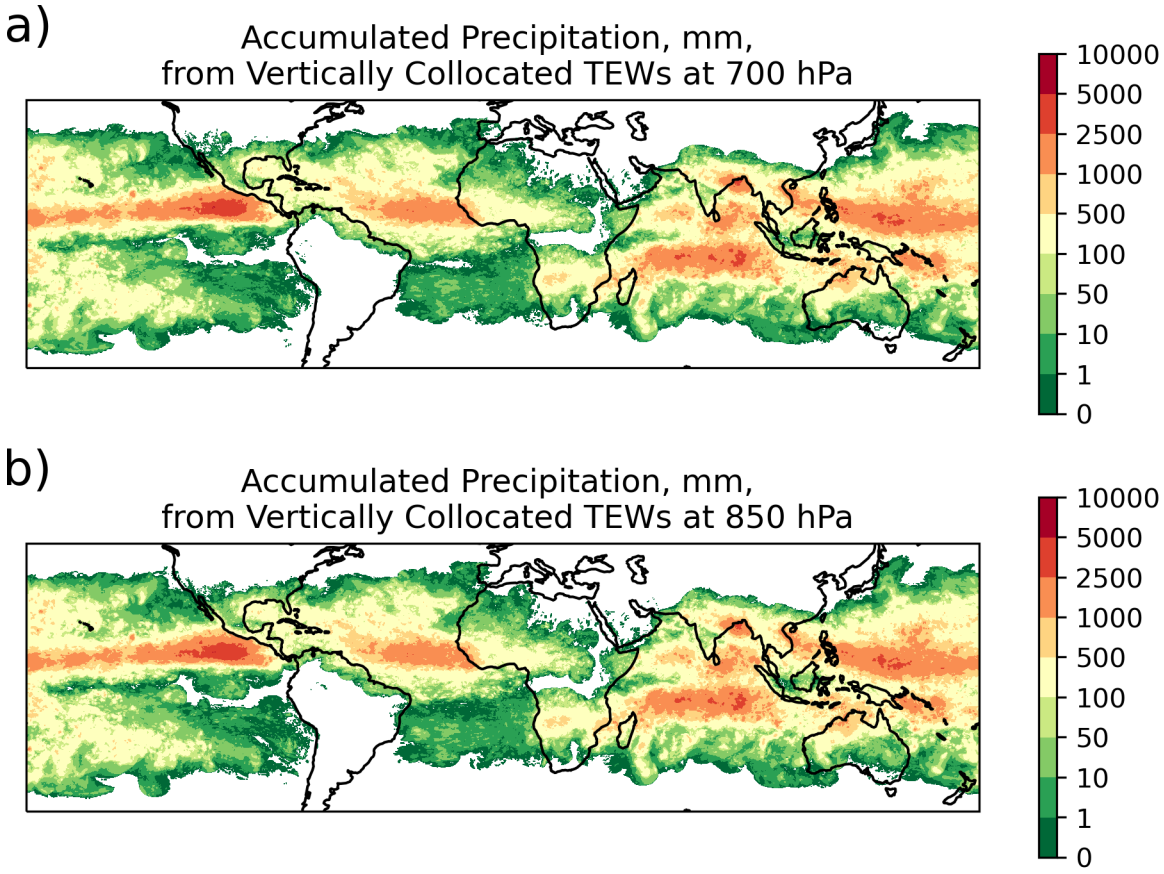

Figure 3.4: Total accumulated precipitation (mm) associated with vertically collocated TEW points tracked at a) 700 hPa and b) 850 hPa, for 2001-2018.

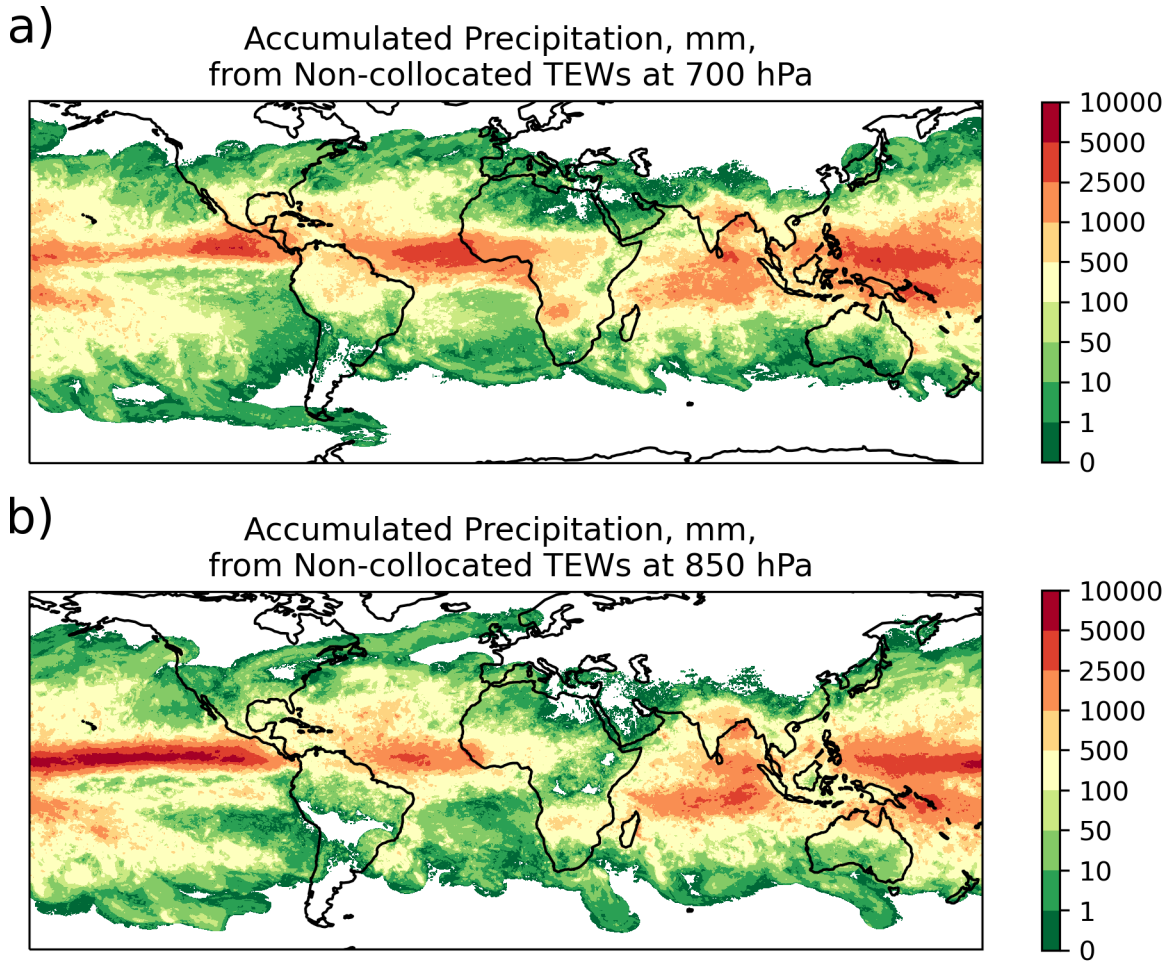

Figure 3.5: Total accumulated precipitation (mm) associated with TEW points that were not vertically collocated from a) 700 hPa and b) 700 hPa, for 2001-2018.

associated with TEW points that were not vertically collocated. At 700 hPa, shown in Figure 3.5a, this area nearly bridges the area between the maximum in the North Atlantic and North Pacific along 15°N. Also extending from the precipitation maximum in the North Atlantic, this broad area of increased precipitation also extends northward, and at 850 hPa even starts turning westward. These two different directions may suggest that TEW vertical level, as well as possibly other factors like CV intensity, may influence the propagation direction of the waves.

Comparing Figures 3.6 and 3.7, which show the annual average precipitation from vertically collocated and non-collocated TEW points, non-collocated wave points are associated with the same order of magnitude of precipitation as points that were vertically collocated. In regions and levels where the average precipitation associated with vertically collocated TEW points is 10-50 mm, generally, the precipitation associated with unmatched TEW points is also 10-50 mm, and similarly for other precipitation ranges. The main exception to this observation is in the tropical North Pacific at 850 hPa, where vertically unmatched TEW points are associated with 250-500 mm of precipitation, in contrast to the vertically collocated points, which are only associated with 50-100 mm of precipitation per year on average.

Figures 3.8 and 3.9 show the fraction of total annual precipitation associated with vertically collocated and non-collocated TEW points, respectively. Complementary to the increase in TEW-associated rainfall downstream of coastlines, the areas where TEWs, regardless of whether their points were vertically collocated, are associated with the greatest percent of rainfall are also over water, downstream of the coastlines and at latitudes where TEWs occur. TEWs crossing from land to ocean, as well as precursor systems like MCSs, may be tapping into additional maritime moisture, yielding increased rainfall.

Vertically collocated AEW points over land, regardless of level and whether they are northern or southern track, are associated with 5% or less of the total annual rainfall. AEW points over land that were not vertically collocated, however, show contributions between

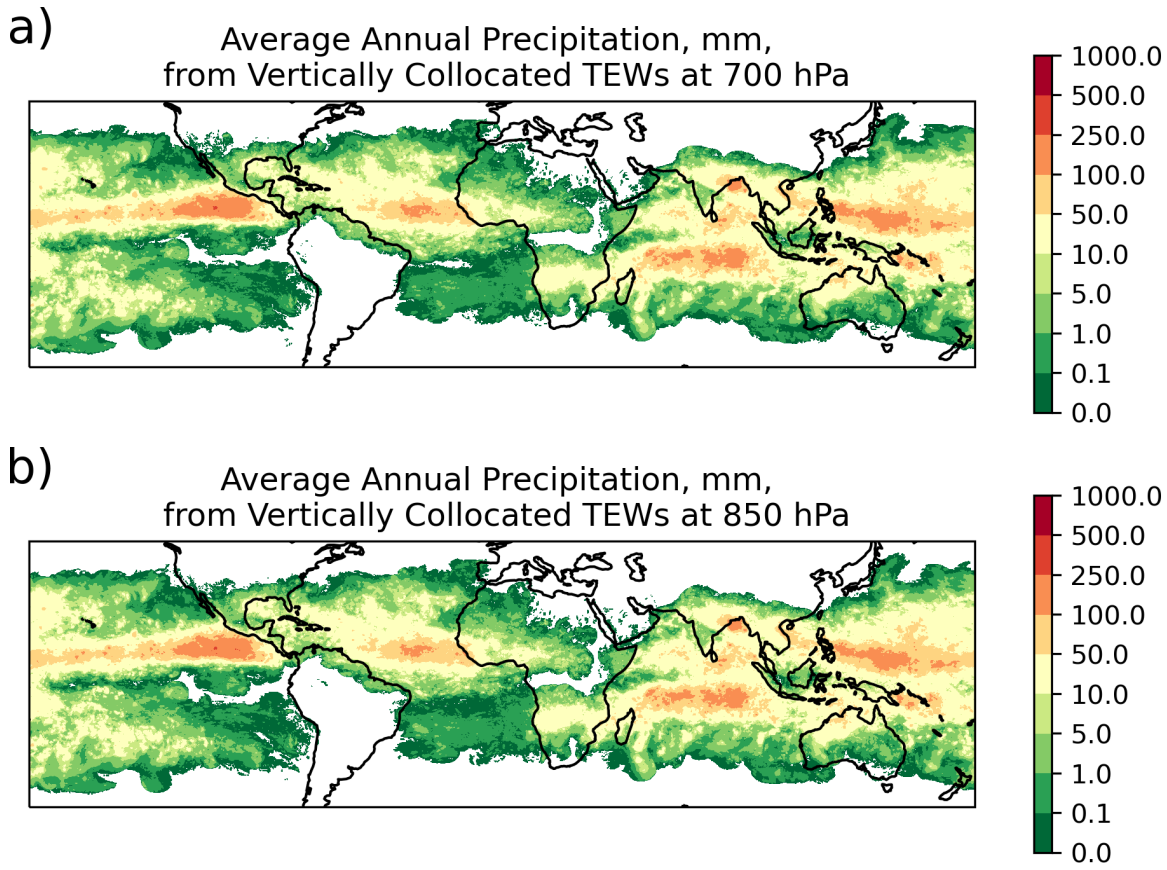

Figure 3.6: Average annual precipitation (mm) associated with vertically collocated TEW points tracked at a) 700 hPa and b) 850 hPa, for 2001-2018.

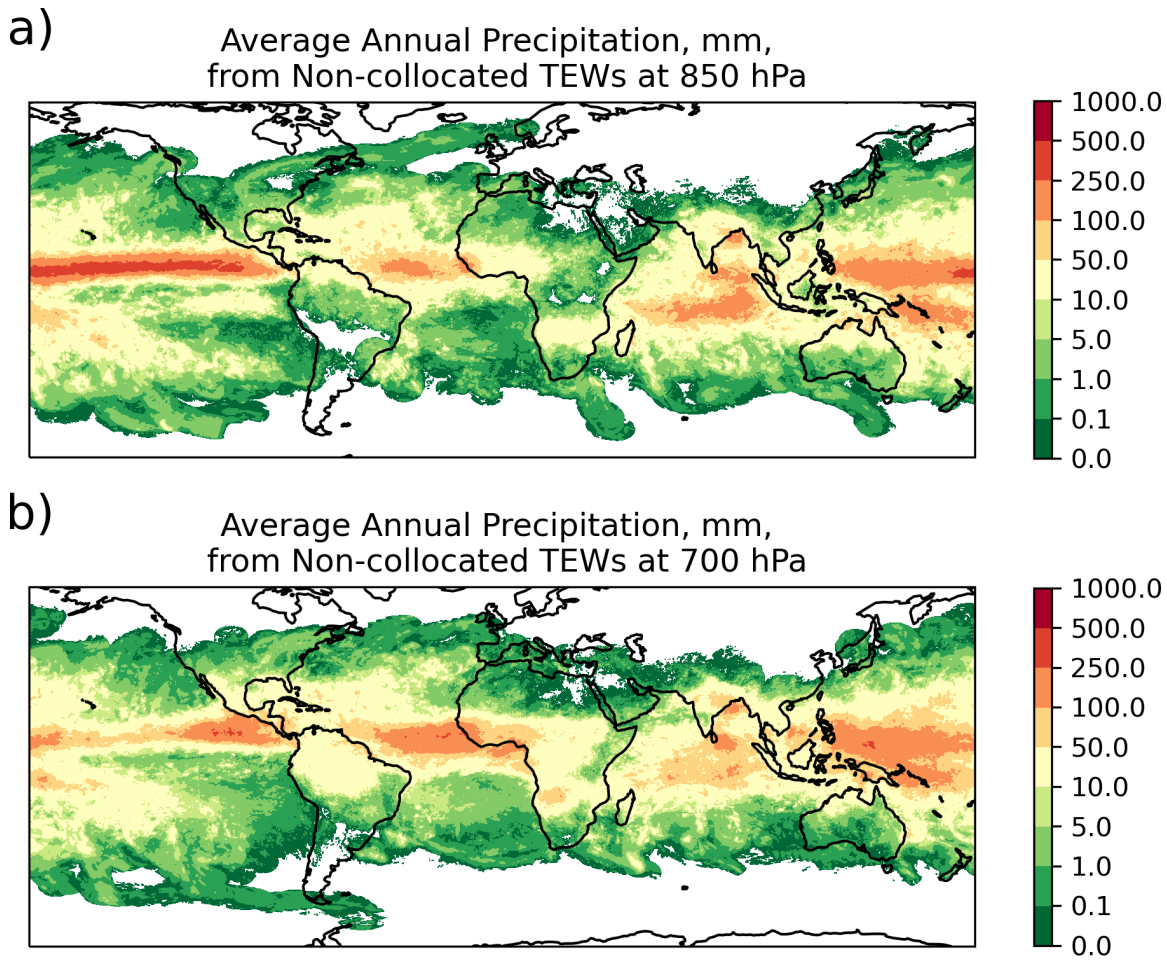

Figure 3.7: Average annual precipitation (mm) associated with TEW points that were not vertically collocated from a) 700 hPa and b) 700 hPa, for 2001-2018.

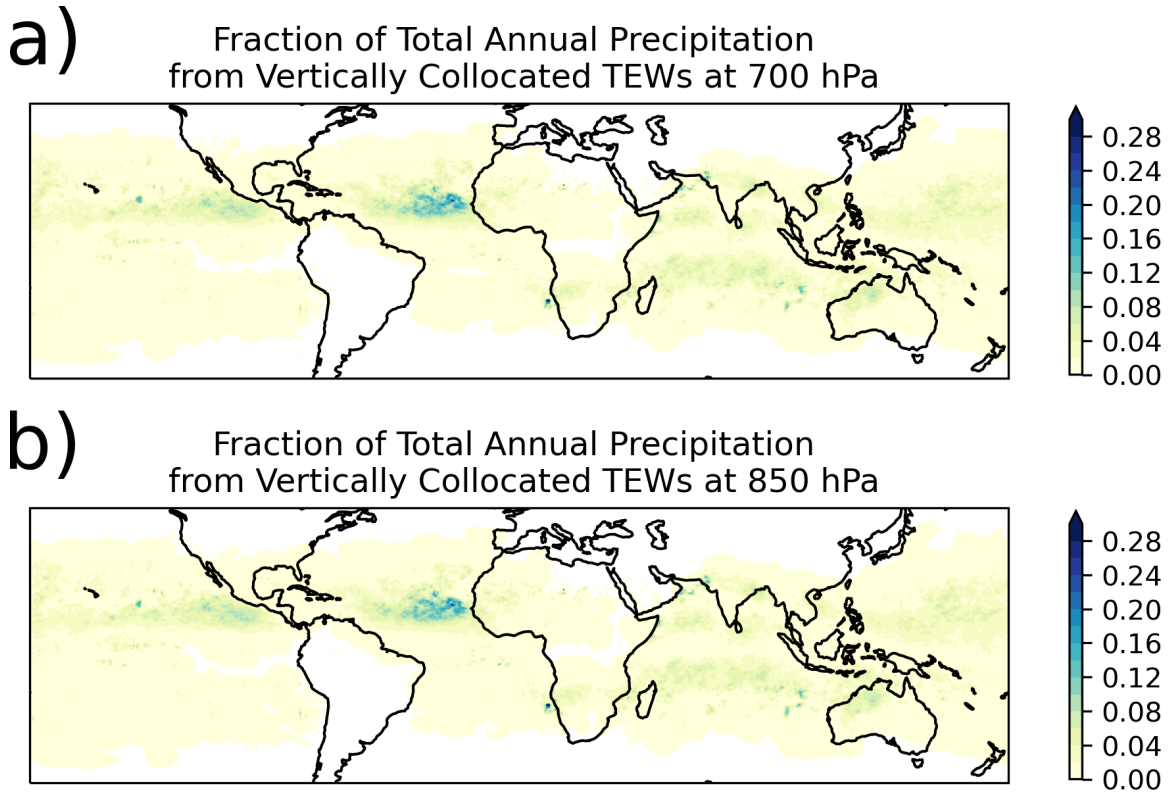

Figure 3.8: Fraction of the annual precipitation associated with vertically collocated TEW points tracked at a) 700 hPa and b) 850 hPa, for 2001-2018.

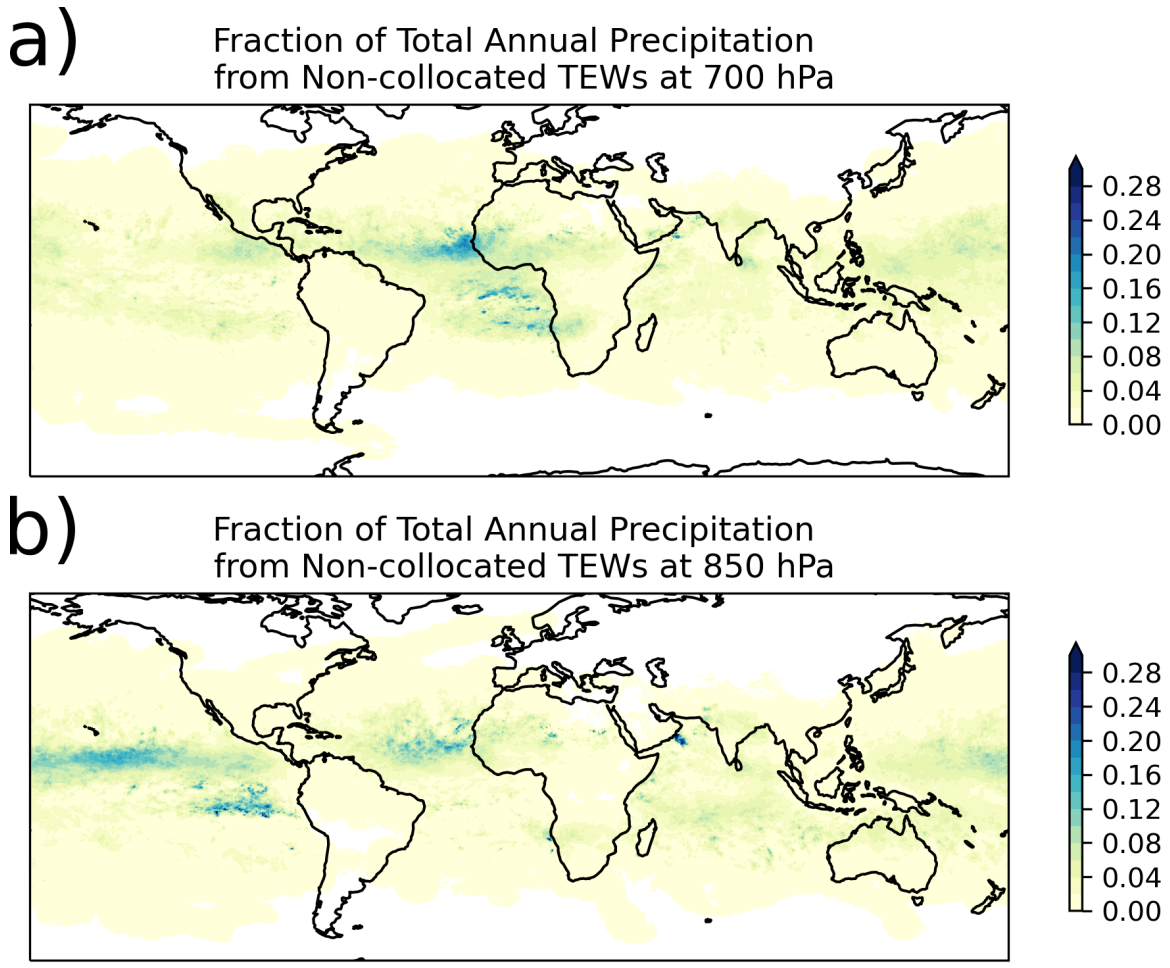

Figure 3.9: Fraction of the annual precipitation associated with TEW points that were not vertically collocated from a) 700 hPa and b) 700 hPa, for 2001-2018.

4-10%, with some locally higher values, along both tracks. Downstream over the tropical Atlantic Ocean, however, those contributions increase to 15-25% for both vertically collocated and non-collocated TEWs, upwards to 30% in some small regions.

Despite an annual average TEW-associated rainfall of 50-250 mm in the Bay of Bengal and inland into India and Bangladesh, both for vertically collocated and non-collocated TEW points, the fraction of the total annual precipitation associated with either category, at any level, is only 4-10%. In contrast, across northern Australia, where the precipitation associated with both collocated and non-collcated TEW points is only 10-50 mm, vertically collocated TEWs are associated with 8-16% of the total annual precipitation, and non-collocated TEWs are associated with an additional 4-10%.

The similar absolute rain contributions and fractions of total annual precipitation associated with vertically collocated and non-collocated TEW points does not mean that the two categories of TEW points have similar amounts of rain associated with each wave, however. As noted in Table 2.2, there 2.5-6 times as many unmatched TEW points as there are vertically collocated points, depending on the level and hemisphere combination in question. Therefore, vertically collocated TEW points are associated with as much rain as the non-collocated points, despite being vastly outnumbered, underlining the potential importance of vertically collocated waves for tropical precipitation.

Finally, Figures 3.10 and 3.11 show the fraction of TEW-associated precipitation associated with vertically collocated and non-collocated TEWs. Across much of the tropics, collocated and non-collocated TEWs are both associated with 40-60% of the total TEW precipitation. Poleward of 35° in each hemisphere, with a few exceptions in the southern Pacific Ocean, over 90% of TEW-associated precipitation is from non-collocated TEW points.

In some cases, collocated TEW points are associated with significantly more precipitation than non-collocated points. In southeast Asia, where the annual average TEW-associated precipitation is 10-50 mm, for collocated TEW points and 1-50 mm for non-collocated

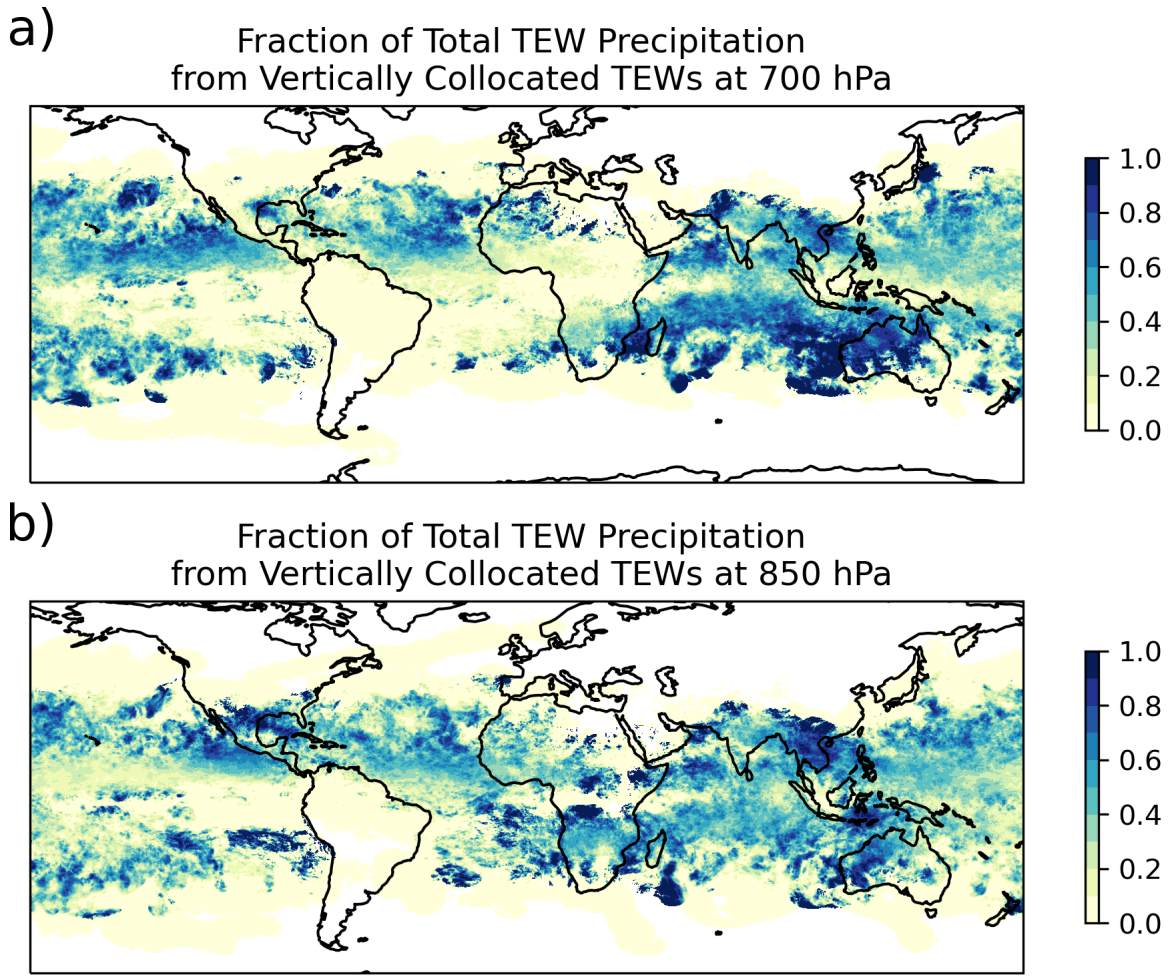

Figure 3.10: Fraction of the total TEW-associated precipitation associated with vertically collocated TEW points tracked at a) 700 hPa and b) 850 hPa, for 2001-2018.

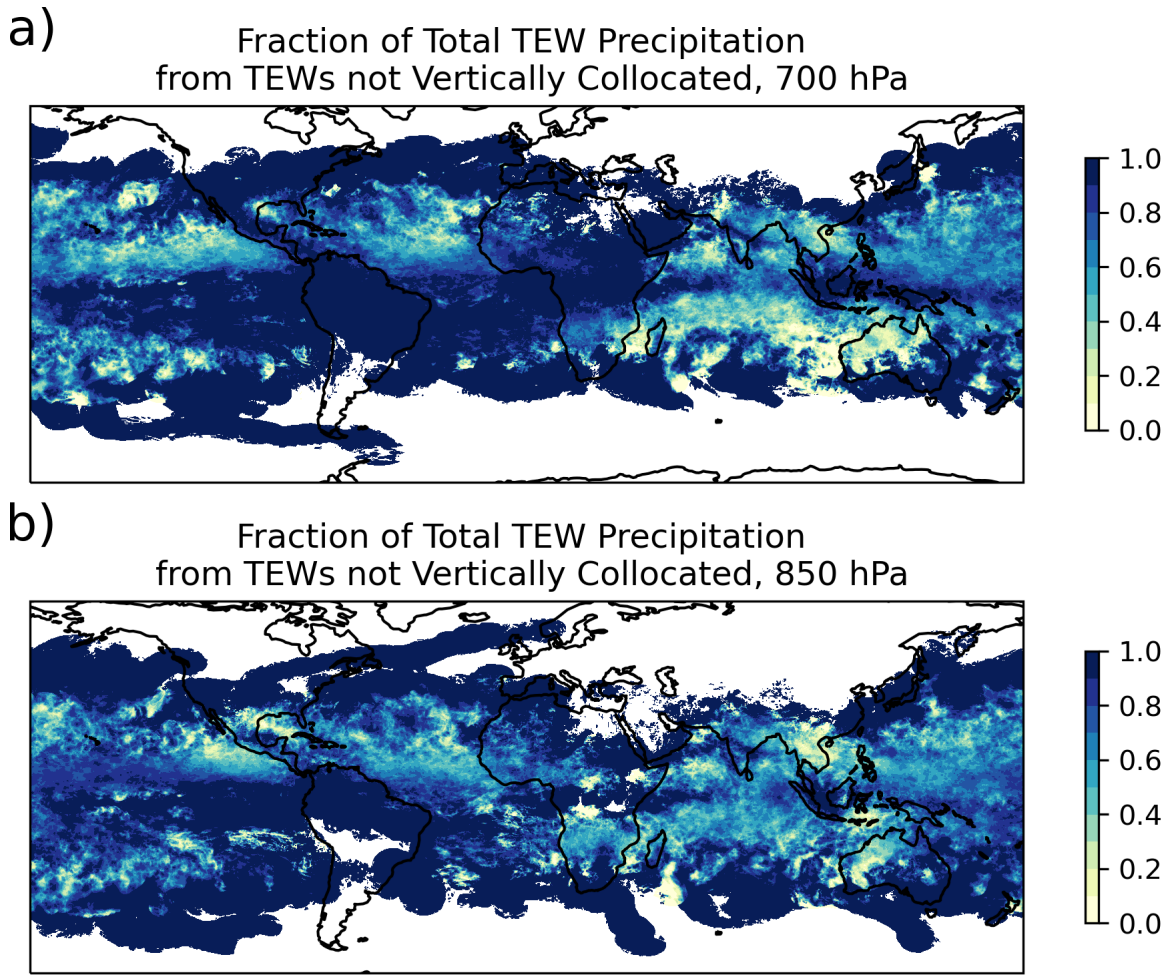

Figure 3.11: Fraction of the annual precipitation (mm) associated with TEW points that were not vertically collocated from a) 700 hPa and b) 700 hPa, for 2001-2018.

points, depending on the level, this is 70-100% of the TEW-associated precipitation. Similarly, across the Australian Outback between 25-30°S, where annual average TEW-associated precipitation is only 1-10 mm, 60-100% of this precipitation is associated with vertically collocated TEWs. The differences between the amounts of precipitation associated with vertically collocated and non-collocated TEWs suggests differences in the precipitation structures for these categories of waves. To better examine this, a wave-centered approach will be more useful

3.2.2 Wave-centered Composites

As seen in the prior section, the precipitation associated with TEWs varies not only region and TEW frequency, but also by whether the wave was identifiable at both 850 and 700 hPa, or only at one level. Comparing the precipitation associated collocated and non-collocated waves in particular is complicated by the different numbers of waves that fall into each category. Instead, by averaging at each grid point in the 500 km radius circle, we can create composites of the precipitation structure around TEWs. Then, looking at the composite precipitation around the CV center, we can look for differences in magnitude and structure without the different number of waves confounding the analysis.

Because the vorticity structures are mirrored between the NH and SH, and the previous plots suggest differences between waves identified at 850 hPa and 700 hPa, the composites shown in Figure 3.12 are separated by level and hemisphere. The track points and associated precipitation in these figures have not been separated by whether or not the track point was collocated or not.

On average, TEWs identified at 850 hPa, regardless of hemisphere, shown in 3.12a and c, were associated with peak rain rates of 0.5-0.6 mm/hr, which is greater than the maximum rain rates associated with at 700 hPa, shown in 3.12 b and d, of 0.3-0.4 mm/hr. Then, at each level, NH TEWs were associated with more rain than SH TEWs at the same level, with NH

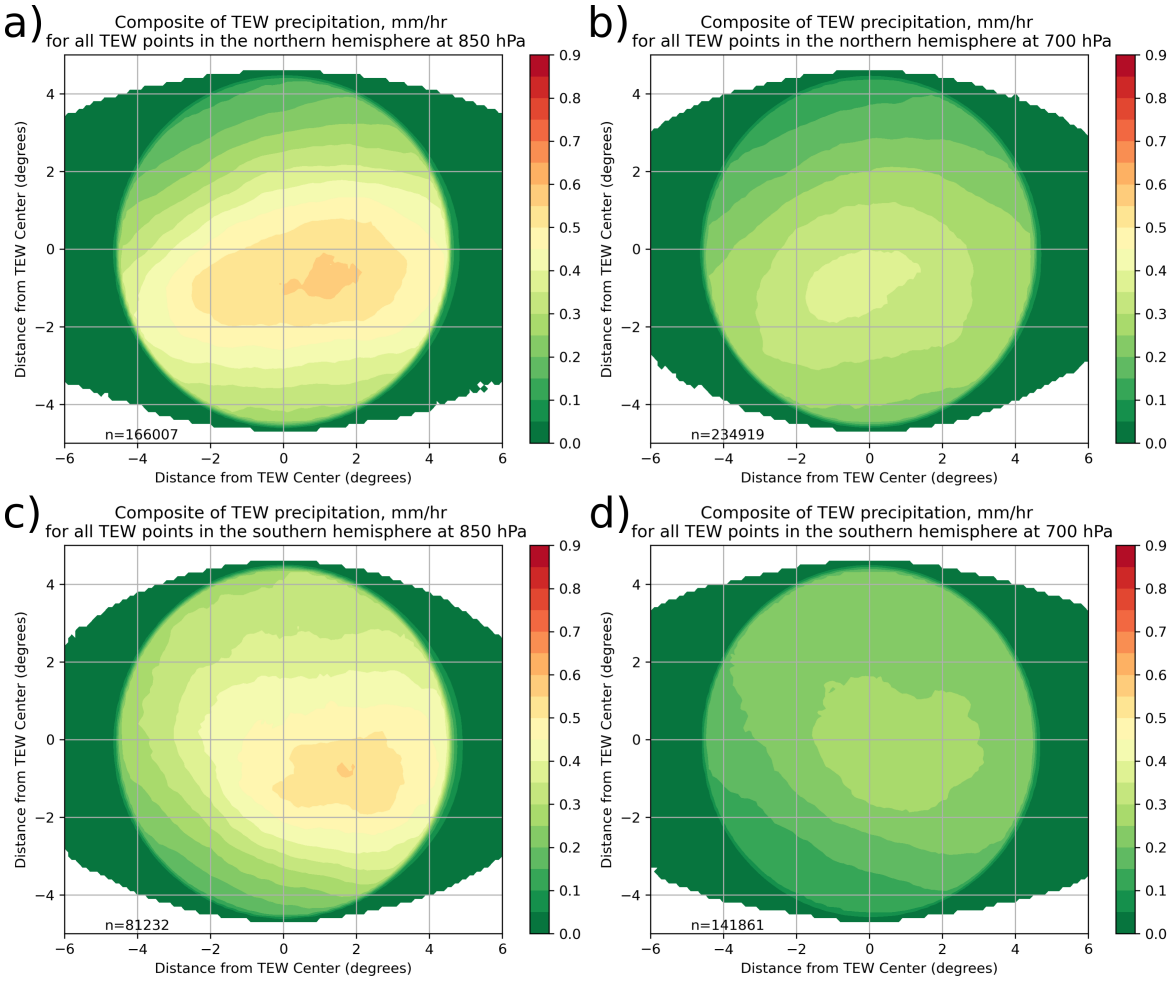

Figure 3.12: Composite of precipitation, mm/hr, associated with TEWs identified a) in the NH at 850 hPa, b) in the NH at 700 hPa, c) in the SH at 850 hPa, and d) in the SH at 700 hPa in the years 2001-2018.

850 hPa TEWs having a broader area with the maximum rain rate of 0.55-0.6 mm/hr than SH 850 hPa TEWs. At 700 hPa, NH TEWs had a maximum average rain rate of 0.35-0.4 mm/hr, while the SH TEWs at that level have an maximum average rain rate of 0.25-0.3 mm/hr.

Despite the different magnitudes of precipitation for the different composites, there are some common features shared between levels and hemispheres. Focusing on the shape and location of the features, some broad similarities exist. All four composites, feature a similar gradient poleward of the area of maximum precipitation. This gradient is at an angle that leads the meridian along which the TEW center is located. Additionally, the gradient in the equatorward direction, in addition to being more zonally oriented, is weaker, suggesting a broader area of light precipitation equatorward of the main precipitation core.

For waves identified in the NH, regardless of level, the peak precipitation is on average 1-2° equatorward of the wave center, while in SH TEWs the peak is located poleward by approximately the same amount. Comparing the levels, however, the precipitation associated with TEWs identified at 850 hPa lags the CV center by approximately 2° of longitude, while the precipitation associated with TEWs identified 700 hPa is more centered on the CV maximum.

The composite variances for these plots, shown in Figure 3.13, follow similar spatial patterns to the composite means, with the maximum variance located in the same areas as the maximum precipitation for each level and hemisphere combination discussed above. However, the composite variance is not as coherent, with multiple centers present in each of the panels. More interestingly though, the variances, which for 850 hPa TEWs maximizes between 5.5 and 6 mm^2/hr^2 in panels a and c of Figure 3.13 and between 2 and 3.5 mm^2/hr^2 for the 700 hPa TEWs in panels b and d, greatly exceeds the mean rain rates shown in Figure 3.12, suggesting that the composite mean precipitation from all TEWs in a given hemisphere and level combination is too broad of a category with which to composite for meaningful results.

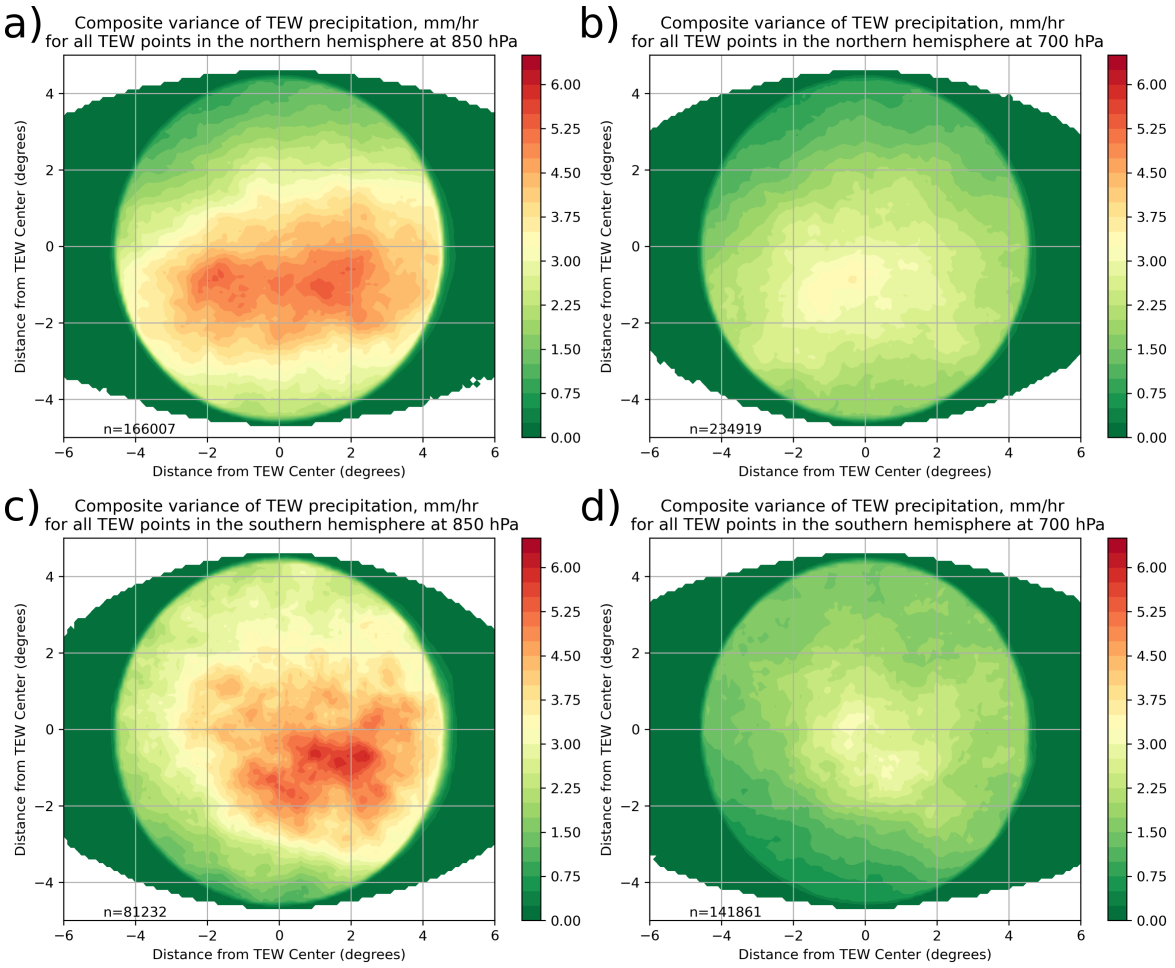

Figure 3.13: Composite variance in precipitation associated with TEWs identified a) in the NH at 850 hPa, b) in the NH at 700 hPa, c) in the SH at 850 hPa, and d) in the SH at 700 hPa.

To this end, instead of compositing all TEW points, we can instead composite the vertically collocated and non-collocated points separately. This allows for a comparison of the precipitation structures between the two subgroups of TEW.

The composites for vertically collocated TEWs are shown in Figure 3.14. Like the composites for all wave points, there is a broad tapering of the precipitation poleward of the TEW center, and an angle to the gradient in the poleward direction. However, the structures in these composites are more similar to each other, with the maximum in precipitation covering an area spanning 4° of longitude, centered on the track point at the CV center of the TEW for all of these composites of vertically collocated waves. The latitudinal extent of the maxima is also similar, approximately 2-3°. However, like in the all-point composites from Figure 3.12, the precipitation associated with NH TEWs tends to be located equatorward of the center of the CV maximum, while precipitation associated with the SH waves tends to exist more poleward of the CV center.

Compared to the composites of all TEW points in Figure 3.12, the vertically collocated TEWs are additionally associated with higher rain rates. In all of the composites from vertically collocated points, the mean rain rate in the core areas described above exceeds 0.6 mm/hr. In contrast with the composites of all wave points, the vertically collocated SH points have higher mean rain rates than the NH points, with vertically collocated points at 700 hPa in the SH exhibiting rain rates between 0.85-0.9 mm/hr.

Figure 3.15 shows the variance for the composite precipitation associated with vertically collocated TEW points. The variance in the strucutre associated with vertically collocated TEWs is, in all four panels, at most 1 mm^2/hr^2, a large reduction in variance compared to the composite from all TEW points. The composite variance in associated precipitation for vertically matched TEW points additionally has a less irregular structure than the variance for all TEW points. For all level and hemisphere combinations, the contours are smoother,

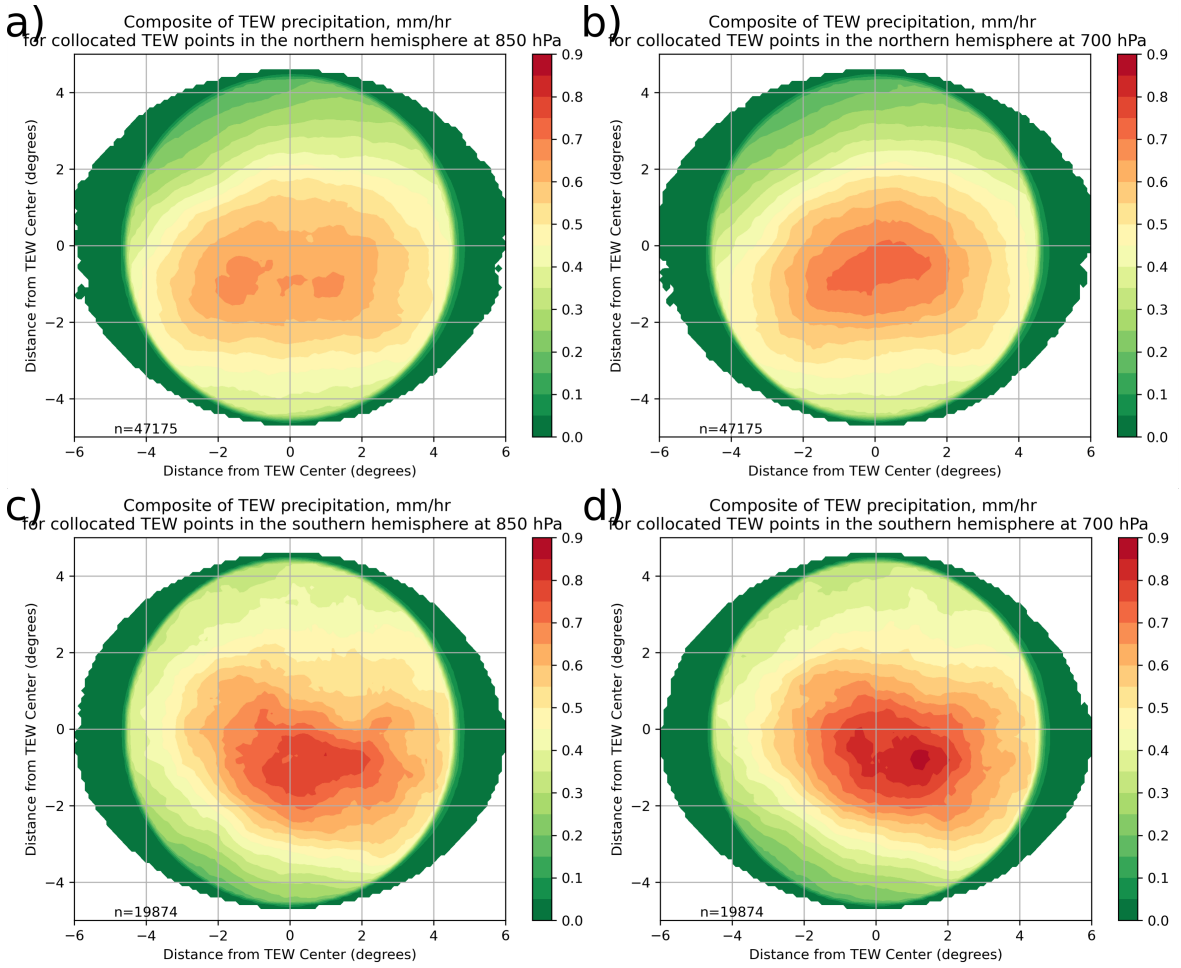

Figure 3.14: Composite precipitation rates, mm/hr, associated with vertically collocated TEW points identified a) in the NH at 850 hPa, b) in the NH at 700 hPa, c) in the SH at 850 hPa, and d) in the SH at 700 hPa.

and have only one center, in contrast with the composite variance from all TEW points, where the variance was multi-centered and had more jagged contours.

In contrast to the peak precipitation in the composite means of the vertically collocated TEW points, the composite means of unmatched TEW points, shown in Figure 3.16, feature lower amounts of precipitation than either the composites for all waves or vertically collocated TEWs. As unmatched points compose a larger percent of the total number of TEW points, these unmatched composites are structurally more similar to the composites of all points from Figure 3.12. Here, the precipitation associated with TEWs identified at 850 hPa lags the CV center by approximately 2°. Precipitation associated with TEWs in the NH at 700 hPa is, by contrast, broadly near the center and ahead of the CV center. Interestingly, there is no distinct precipitation center for the precipitation associated with SH TEWs identified at 700 hPa.

In these composites of unmatched TEW points, wave points at 850 hPa have higher rain rates than those at 700 hPa, with the maximum mean precipitation rate for the 850 hPa waves reaching 0.55 mm/hr, while the highest mean precipitation rate for 700 hPa points is 0.2-0.25 mm/hr.

Despite the similarities in shape between the composites of all TEW points and the unmatched TEW points, the composite variance of the precipitation associated with unmatched TEWs, shown in Figure 3.17, is as low as or lower than the composite variance of the vertically matched TEWs. For TEW points at 850 hPa in the SH that were not vertically collocated, shown in Figure 3.17d, the variance across the entire area is at most 0.25 mm^2/hr^2

With the low variance in both vertically collocated and non-collocated TEW points, this leads to the conclusion that more vertically coherent TEWs can be associated with increased and more organized precipitation, while TEWs that are less vertically coherent, either because the wave is only present at one level, or because the wave is too vertically tilted, are associated with less precipitation. The increased organization of the precipitation suggests

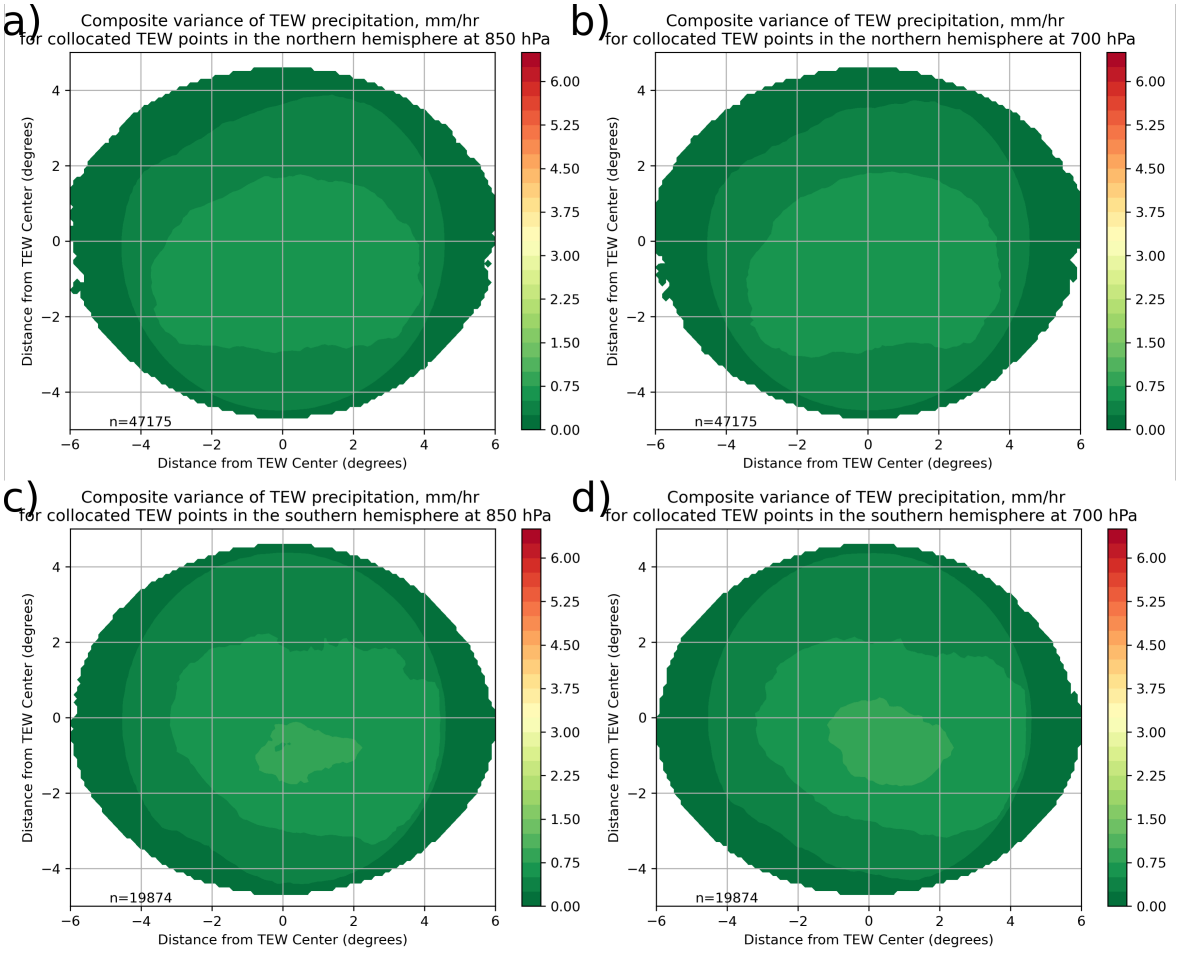

Figure 3.15: Composite variance in precipitation associated with vertically collocated TEW points identified a) in the NH at 850 hPa, b) in the NH at 700 hPa, c) in the SH at 850 hPa, and d) in the SH at 700 hPa.

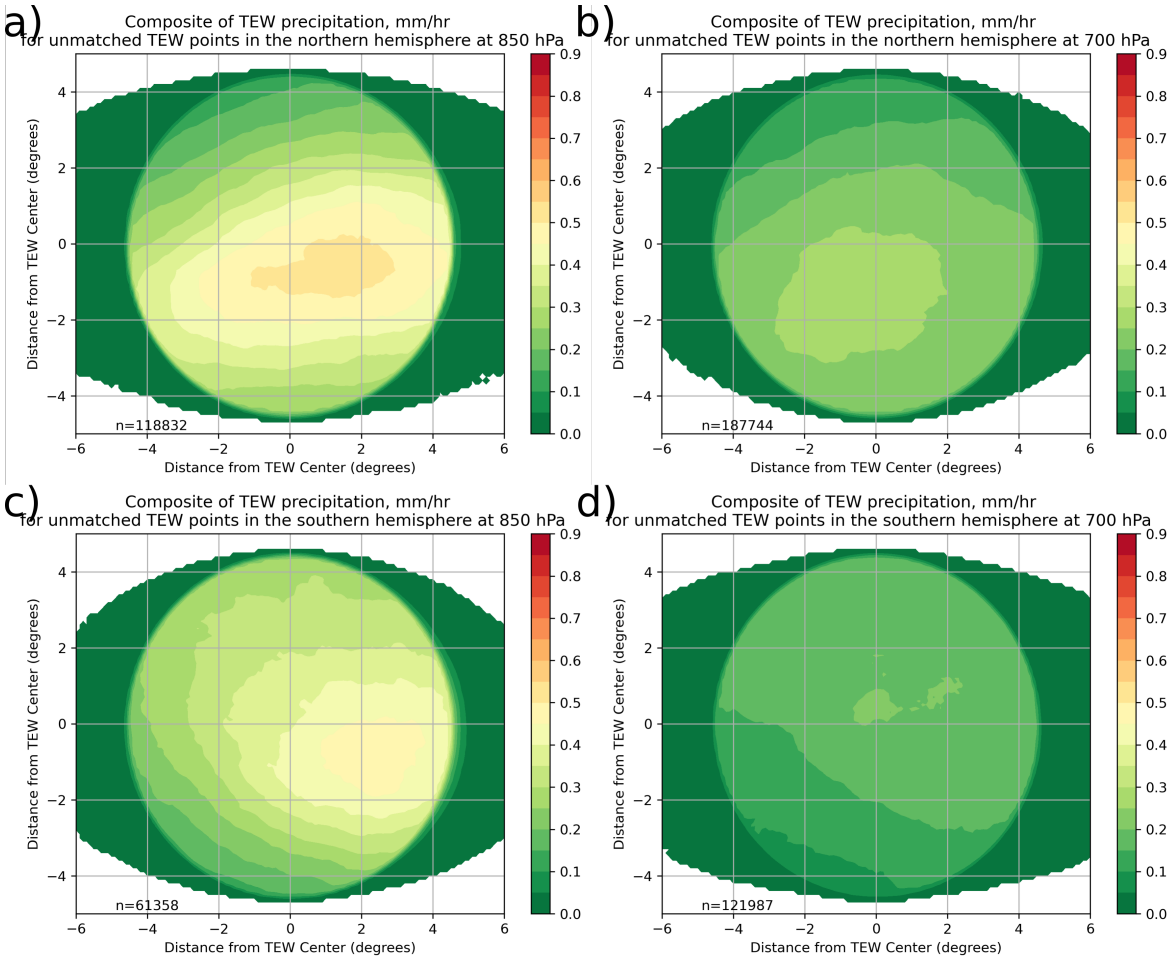

Figure 3.16: Composite precipitation rates, mm/hr, associated with TEW points that were not vertically collocated from a) the NH at 850 hPa, b) the NH at 700 hPa, c) the SH at 850 hPa, and d) the SH at 700 hPa.

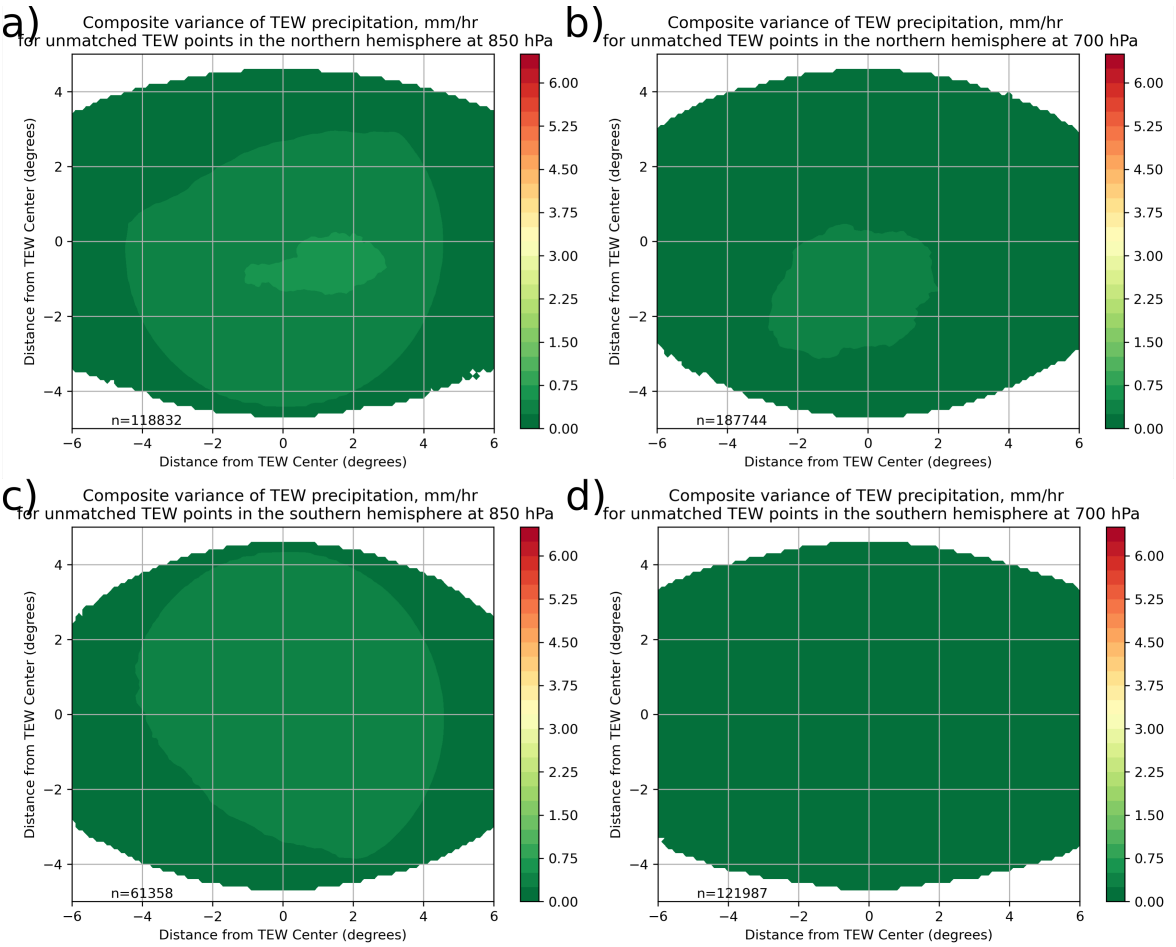

Figure 3.17: Composite variance in precipitation associated with TEW points that were not vertically collocated from a) the NH at 850 hPa, b) the NH at 700 hPa, c) the SH at 850 hPa, and d) the SH at 700 hPa.

that waves where significant cyclonic CV is present at both 850 and 700 hPa have more organized structures that are able to create and sustain more intense rainfall, namely increased organized convection. Physically, this makes sense, as the low-level CV may contribute to instability through the column.

Chapter 4

Conclusion

The goals of this project were to develop a global climatology of TEWs and to use that database to study how TEWs contribute to precipitation across the tropics. Developing a global climatology fills a gap in current literature, where varying methods across regional studies complicate attempts to compare results between regions. A global TEW database also creates the opportunity to study the precipitation associated with TEWs from a broader perspective than regional studies. The results presented here only scratch the surface of what we can learn from the wave database, and additional avenues of potential investigation will be outlined below.

4.1 Summary

To identify TEWs globally, we used TRACK to identify cyclonic CV maxima (minima for the SH), and then developed a set of criteria to filter the TRACK output for meaningful results. Our criteria were:

1. The tracked CV feature must have originated equatorward of 40°,

2. The tracked feature must travel at least 15° from west to east within the tropics

While some short-lived TEWs may have been removed by this method, 38723 TEW tracks were identified between 850 and 700 hPa across the 38 years analyzed. After TEWs

were identified, we removed the TC portions of tracks, by matching the TEW tracks against IBTrACS. This removed part or all of slightly more than 2600 tracks at each level.

Tracking TEWs globally and for full calendar years shows that TEWs occur throughout the tropics and at all times of year, but with preferred regions and seasons. When compared with existing regional climatologies (e.g, Belanger et al. 2016; Berry et al. 2012; Thorncroft and Hodges 2001), we have found similar areas of increased TEW activity, such as north Africa and the northern Atlantic Ocean, as well as the eastern North Pacific Ocean. In addition to these known regions of TEW activity, we found additional regional peaks in activity in the southern Atlantic, Pacific, and Indian Oceans.

In each hemisphere, more TEWs occur in that hemisphere's summer and fall months, though the seasonal pattern is more prominent in the NH than in the SH. This pattern exists at both 850 and 700 hPa, despite the fact that there were nearly twice as many waves identified at 700 hPa. Variability exists in the annual counts of TEWs as well, with annual global wave counts varying from 500 to 700 waves per year at 700 hPa, and from 300 to 450 waves per year at 850 hPa. The causes of this variability have not been thoroughly investigated. Theories on potential causes of interannual variability in TEW activity are discussed in Section 4.2.

Across all regions and levels, the waves we have identified have average lifetimes and phase speeds consistent with values from regional studies. As identified in this research, TEWs have an average phase speed near 7.5 ms^{-1}, and propagate on average approximately 3000 km, with little variance between the levels and hemispheres. This lends confidence to our broad definition of a TEW as an area of cyclonic curvature vorticity in the lower levels of the atmosphere that propagates westward in the tropics. This also highlights the need to study TEWs in a global context so that more comparisons can be done.

When measured by the number of collocated points, the greatest TEW collocation occurred in the regions with the greatest TEW activity, particularly the North Atlantic and

eastern North Pacific Oceans, as well as the southern Indian Ocean. In contrast, when measured by percent of points that were vertically collocated, peak regions of vertical collocation broadened, included area over land, and included areas with more modest TEW activity, such as over southern Africa, northwestern Australia, and the northern Indian Ocean.

By associating precipitation within a 500 km radius with the influence of a TEW, we have shown that TEWs can be associated with 25% or more of the total annual precipitation in parts of the tropics in regions where they occur frequently, such as the North Atlantic and North Pacific Oceans. Decomposing these contributions to whether a wave point was vertically collocated or not, vertically collocated TEW points in regions of increased TEW activity during the period 2001-2018, despite accounting for only 27% of the 850 hPa wave points and 17% of the 700 hPa wave points, are associated with 10% of the total annual precipitation from all sources. Vertically collocated TEWs contributed half or more of the total TEW-associated precipitation in many regions, including the Gulf of Mexico, Australia, and southeast Asia. With relatively little variance in the precipitation structures after separating collocated waves, this leads us to the conclusions that

1. TEWs overall are important contributors to total tropical precipitation

2. per wave point, vertically coherent TEWs are outsized contributors when compared to waves that were not vertically collocated

4.2 Future Work

Building off of the work presented here, an obvious extension would be to examine more specific regions using this track database. To our knowledge, there is a lack of in-depth inter-regional comparisons of TEWs and their characteristics, especially comparing more than two regions. Most existing comparisons rely on using AEWs as a point of comparison (e.g.

Dickinson and Molinari 2000; Berry et al. 2012). This global database, which we have shown is able to identify waves in multiple regions and is not affected by irregular return periods, has many potential uses for future regional studies. Using this database, we could compare how wave activity is represented in this database to how wave activity was represented in other studies, such as Dickinson and Molinari (2000), using similar regions. With a global database, we also have the opportunity to compare additional regions that have not been thoroughly studied, such as the southeastern Pacific Ocean and southern Africa.

To further investigate the dynamical structure of TEWs, there are two main directions further work might take. The first would be to apply the methods described in Section 2.1 to additional levels of MERRA-2. This would enable the creation of vertical profiles of CV through the existing 850 or 700 hPa wave track points and the tracking of TEWs at additional levels. With TEW tracks at additional levels, vertical track point matching could be done at those additional levels between the surface and middle levels of the atmosphere, giving detailed information about the tilt of TEWs. The second direction future investigations could take would involve the creation of composites of the dynamical fields from MERRA-2, such as the wind, pressure, and geopotential height fields.

Another opportunity this database of TEW tracks presents is to study how TEWs change throughout their life, both dynamically and in the precipitation. Schlueter et al. (2019b) used OLR to derive wave phases for a variety of tropical waves over northern Africa and the composited rainfall by wave phase and type. Following similar methods, but for CV or TEW-associated precipitation, we could derive wave phases for the TEWs in our database. These wave phases could then serve as another way to compare dynamical and precipitation characteristics of TEWs. Using wave phase may be an interesting way to compare the longest-lived TEWs to those with more average propagation distances.

Location and wave phase are not the only factors that may affect TEWs. Environmental factors surrounding TEWs may also play a part in modulating TEW precipitation, potentially

interacting with the various phases of the TEW life cycle. In a study of the relationship between AEWs and Kelvin waves, Ventrice and Thorncroft (2013) showed that Kelvin waves influence AEW activity. Additionally, Schreck (2015) showed that Kelvin waves have a role in tropical cyclogenesis, and that with TEWs often serve as seed disturbances for TCs. Therefore, studying the interactions between TEWs, Kelvin waves, and other environmental factors may point towards reasons for differences in intensity and precipitation structure of TEWs.

All of these potential directions for future work can be pursued both from a global scale and from a more regional perspective. For example, while CV could be calculated at more levels globally, the global analysis could be complemented by comparing average profiles through TEW points from different regions. The synoptic, regional, and global scales are all related, and this database allows study from all three spatial scales.

At longer time scales, we would also be interested in studying potential causes of interannual variability in TEW activity, as well as if there is any interannual variability in TEW-associated precipitation. Elless and Torn (2019) has theorized that ENSO and other large-scale teleconnections may have an impact on AEW intensity. Dominguez et al. (2020) has found that there are fewer TEWs and less TEW-associated precipitation over northern South America during El Nino years. We would be interested in studying if similar relationships hold for other regions.

In addition to future work that leverages the existing TEW database and TEW-associated precipitation, applying these methods to other datasets could produce valuable comparisons to help identify biases in MERRA-2 and IMERG. Belanger et al. (2016) showed differences in the quantities of TEWs tracked in the western hemisphere between four reanalysis datasets when applying identical methods to each. An obvious choice would be to use the precipitation fields from MERRA-2 to compare to IMERG, but the same methods could be applied

to any reanalysis dataset or even climate models. Climate models may be especially useful for studying the behavior of TEWs in future climate scenarios.

Reference List

Belanger, J. I., M. T. Jelinek, and J. A. Curry, 2016: A climatology of easterly waves in the tropical Western Hemisphere. *Geosci. Data J.*, **3 (2)**, 40–49, doi:10.1002/gdj3.40, URL http://doi.wiley.com/10.1002/gdj3.40.

Berry, G. J., M. J. Reeder, and C. Jakob, 2012: Coherent Synoptic Disturbances in the Australian Monsoon. *Journal of Climate*, **25 (24)**, 8409–8421, doi:10.1175/JCLI-D-12-00143.1, URL https://journals.ametsoc.org/jcli/article/25/24/8409/33672/Coherent-Synoptic-Disturbances-in-the-Australian.

Brammer, A., and C. D. Thorncroft, 2015: Variability and Evolution of African Easterly Wave Structures and Their Relationship with Tropical Cyclogenesis over the Eastern Atlantic. *Monthly Weather Review*, **143 (12)**, 4975–4995, doi:10.1175/MWR-D-15-0106.1, URL https://journals.ametsoc.org/mwr/article/143/12/4975/72006/Variability-and-Evolution-of-African-Easterly-Wave.

Brannan, A. L., and E. R. Martin, 2019: Future characteristics of African Easterly Wave tracks. *Clim Dyn*, **52 (9-10)**, 5567–5584, doi:10.1007/s00382-018-4465-z, URL http://link.springer.com/10.1007/s00382-018-4465-z.

Burpee, R. W., 1972: The Origin and Structure of Easterly Waves in the Lower Troposphere of North Africa. *Journal of the Atmospheric Sciences*, **29 (1)**, 77–90, URL https://journals.ametsoc.org/view/journals/atsc/29/1/1520-0469_1972_029_0077_toasoe_2_0_co_2.xml, publisher: American Meteorological Society Section: Journal of the Atmospheric Sciences.

Carlson, T. N., 1969: Some Remarks on African Disturbances and Their Progress Over the Tropical Atlantic. *Monthly Weather Review*, **97 (10)**, 716–726.

Charney, J. G., and M. E. Stern, 1962: On the Stability of Internal Baroclinic Jets in a Rotating Atmosphere. *Journal of the Atmospheric Sciences*, **19 (2)**, 159–172, doi:10.1175/1520-0469(1962)019⟨0159:OTSOIB⟩2.0.CO;2, URL https://journals.ametsoc.org/view/journals/atsc/19/2/1520-0469_1962_019_0159_otsoib_2_0_co_2.xml, publisher: American Meteorological Society Section: Journal of the Atmospheric Sciences.

Chen, T.-C., 2006: Characteristics of African Easterly Waves Depicted by ECMWF Reanalyses for 1991–2000. *Monthly Weather Review*, **134 (12)**, 3539–3566, doi:10.1175/MWR3259.1, URL https://journals.ametsoc.org/view/journals/mwre/134/12/mwr3259.1.xml, publisher: American Meteorological Society Section: Monthly Weather Review.

Dickinson, M., and J. Molinari, 2000: Climatology of Sign Reversals of the Meridional Potential Vorticity Gradient over Africa and Australia. *Monthly Weather Review*, **128**, 11.

Dominguez, C., J. M. Done, and C. L. Bruyère, 2020: Easterly wave contributions to seasonal rainfall over the tropical Americas in observations and a regional climate model. *Clim Dyn*, **54 (1)**, 191–209, doi:10.1007/s00382-019-04996-7, URL https://doi.org/10.1007/s00382-019-04996-7.

Eliassen, A., 1983: The Charney-Stern theorem on barotropic-baroclinic instability. *Pure and Applied Geophysics PAGEOPH*, **121 (3)**, 563–572, doi:10.1007/BF02590155, URL http://link.springer.com/10.1007/BF02590155.

Elless, T. J., and R. D. Torn, 2019: Investigating the Factors That Contribute to African Easterly Wave Intensity Forecast Uncertainty in the ECMWF Ensemble Prediction System. *Monthly Weather Review*, **147 (5)**, 1679–1698, doi:10.1175/MWR-D-18-0071.1, URL

https://journals.ametsoc.org/view/journals/mwre/147/5/mwr-d-18-0071.1.xml, publisher: American Meteorological Society Section: Monthly Weather Review.

Engel, T., A. H. Fink, P. Knippertz, G. Pante, and J. Bliefernicht, 2017: Extreme Precipitation in the West African Cities of Dakar and Ouagadougou: Atmospheric Dynamics and Implications for Flood Risk Assessments. *Journal of Hydrometeorology*, **18 (11)**, 2937–2957, doi:10.1175/JHM-D-16-0218.1, URL https://journals.ametsoc.org/view/journals/hydr/18/11/jhm-d-16-0218_1.xml, publisher: American Meteorological Society Section: Journal of Hydrometeorology.

Fink, A. H., and A. Reiner, 2003: Spatiotemporal variability of the relation between African Easterly Waves and West African Squall Lines in 1998 and 1999. *J. Geophys. Res.*, **108 (D11)**, 4332, doi:10.1029/2002JD002816, URL http://doi.wiley.com/10.1029/2002JD002816.

Fink, A. H., D. G. Vincent, P. M. Reiner, and P. Speth, 2004: Mean State and Wave Disturbances during Phases I, II, and III of GATE Based on ERA-40. *Monthly Weather Review*, **132 (7)**, 1661–1683, doi:10.1175/1520-0493(2004)132⟨1661:MSAWDD⟩2.0.CO;2, URL https://journals.ametsoc.org/view/journals/mwre/132/7/1520-0493_2004_132_1661_msawdd_2.0.co_2.xml, publisher: American Meteorological Society Section: Monthly Weather Review.

Fukutomi, Y., 2019: Tropical Synoptic-Scale Waves Propagating Across the Maritime Continent and Northern Australia. *J. Geophys. Res. Atmos.*, **124 (14)**, 7665–7682, doi:10.1029/2018JD029795, URL https://onlinelibrary.wiley.com/doi/abs/10.1029/2018JD029795.

Fuller, R. D., and D. J. Stensrud, 2000: The Relationship between Tropical Easterly Waves and Surges over the Gulf of California during the North American Monsoon. *Monthly Weather Review*, **128**, 7.

GSFC, P. P. S. P. A. N., 2019: GPM IMERG Final Precipitation L3 Half Hourly 0.1 degree x 0.1 degree V06. NASA Goddard Earth Sciences Data and Information Services Center, URL https://disc.gsfc.nasa.gov/datacollection/GPM_3IMERGHH_06.html, type: dataset, doi:10.5067/GPM/IMERG/3B-HH/06.

Hodges, K., A. Cobb, and P. L. Vidale, 2017: How Well Are Tropical Cyclones Represented in Reanalysis Datasets? *J. Climate*, **30 (14)**, 5243–5264, doi:10.1175/JCLI-D-16-0557.1, URL http://journals.ametsoc.org/doi/10.1175/JCLI-D-16-0557.1.

Hodges, K. I., 1995: Feature Tracking on a Unit Sphere. *Monthly Weather Review*, **123**, 3458–3465.

Hodges, K. I., B. J. Hoskins, J. Boyle, and C. Thorncroft, 2003: A Comparison of Recent Reanalysis Datasets Using Objective Feature Tracking: Storm Tracks and Tropical Easterly Waves. *Monthly Weather Review*, **131**, 26.

Hsieh, J.-S., and K. H. Cook, 2005: Generation of African Easterly Wave Disturbances: Relationship to the African Easterly Jet. *Monthly Weather Review*, **133 (5)**, 1311–1327, doi:10.1175/MWR2916.1, URL https://journals.ametsoc.org/mwr/article/133/5/1311/67510/Generation-of-African-Easterly-Wave-Disturbances.

Hurley, J. V., and W. R. Boos, 2015: A global climatology of monsoon low-pressure systems: Global Climatology of Monsoon Low-Pressure Systems. *Q.J.R. Meteorol. Soc.*, **141 (689)**, 1049–1064, doi:10.1002/qj.2447, URL http://doi.wiley.com/10.1002/qj.2447.

Jiang, H., and E. J. Zipser, 2010: Contribution of Tropical Cyclones to the Global Precipitation from Eight Seasons of TRMM Data: Regional, Seasonal, and Interannual Variations. *Journal of Climate*, **23 (6)**, 1526–1543, doi:10.1175/2009JCLI3303.1, URL https://journals.ametsoc.org/jcli/article/23/6/1526/32968/Contribution-of-Tropical-Cyclones-to-the-Global.

Knapp, K. R., H. J. Diamond, J. P. Kossin, M. C. Kruk, and C. J. Schreck, 2018: International Best Track Archive for Climate Stewardship (IBTrACS) Project, Version 4. NOAA National Centers for Environmental Information, URL https://data.nodc.noaa.gov/cgi-bin/iso?id=gov.noaa.ncdc:C01552, type: dataset, doi:10.25921/82TY-9E16.

Ladwig, W. C., and D. J. Stensrud, 2009: Relationship between Tropical Easterly Waves and Precipitation during the North American Monsoon. *Journal of Climate*, **22 (2)**, 258–271, doi:10.1175/2008JCLI2241.1, URL https://journals.ametsoc.org/jcli/article/22/2/258/31886/Relationship-between-Tropical-Easterly-Waves-and.

Landsea, C. W., and W. M. Gray, 1992: The Strong Association between Western Sahelian Monsoon Rainfall and Intense Atlantic Hurricanes. *J. Climate*, **5 (5)**, 435–453, doi:https://doi.org/10.1175/1520-0442(1992)005%3C0435:TSABWS%3E2.0.CO;2.

Molinari, J., D. Vollaro, S. Skubis, and M. Dickinson, 2000: Origins and Mechanisms of Eastern Pacific Tropical Cyclogenesis: A Case Study. *Monthly Weather Review*, **128**, 15.

Moron, V., A. W. Robertson, M. N. Ward, and O. Ndiaye, 2008: Weather Types and Rainfall over Senegal. Part I: Observational Analysis. *Journal of Climate*, **21 (2)**, 266–287, doi:10.1175/2007JCLI1601.1, URL https://journals.ametsoc.org/view/journals/clim/21/2/2007jcli1601.1.xml, publisher: American Meteorological Society Section: Journal of Climate.

Office, G. M. A. A., and S. Pawson, 2015: MERRA-2 inst3_3d_asm_np: 3d,3-Hourly,Instantaneous,Pressure-Level,Assimilation,Assimilated Meteorological Fields V5.12.4. NASA Goddard Earth Sciences Data and Information Services Center, URL https://disc.gsfc.nasa.gov/datacollection/M2I3NPASM_5.12.4.html, type: dataset, doi:10.5067/QBZ6MG944HW0.

Pasch, R. J., and L. A. Avila, 1994: Atlantic Tropical Systems of 1992. *Mon. Wea. Rev.*, **122 (3)**, 539–548, doi:https://doi.org/10.1175/1520-0493(1994)122%3C0539:ATSO%3E2.0.CO;2.

Reed, R. J., A. Hollingsworth, W. A. Heckley, and F. Delsol, 1988: An Evaluation of the Performance of the ECMWF Operational System in Analyzing and Forecasting Easterly Wave Disturbances over Africa and the Tropical Atlantic. *Mon. Wea. Rev.*, **116**, 824–865.

Reed, R. J., D. C. Norquist, and E. E. Recker, 1977: The Structure and Properties of African Wave Disturbances as Observed During Phase III of GATE. *Mon. Wea. Rev.*, **105**, 317–333.

Schlueter, A., A. H. Fink, and P. Knippertz, 2019a: A Systematic Comparison of Tropical Waves over Northern Africa. Part II: Dynamics and Thermodynamics. *Journal of Climate*, **32 (9)**, 2605–2625, doi:10.1175/JCLI-D-18-0651.1, URL https://journals.ametsoc.org/jcli/article/32/9/2605/344173/A-Systematic-Comparison-of-Tropical-Waves-over.

Schlueter, A., A. H. Fink, P. Knippertz, and P. Vogel, 2019b: A Systematic Comparison of Tropical Waves over Northern Africa. Part I: Influence on Rainfall. *Journal of Climate*, **32 (5)**, 1501–1523, doi:10.1175/JCLI-D-18-0173.1, URL http://journals.ametsoc.org/doi/10.1175/JCLI-D-18-0173.1.

Schreck, C. J., 2015: Kelvin Waves and Tropical Cyclogenesis: A Global Survey. *Monthly Weather Review*, **143 (10)**, 3996–4011, doi:10.1175/MWR-D-15-0111.1, URL https://journals.ametsoc.org/view/journals/mwre/143/10/mwr-d-15-0111.1.xml, publisher: American Meteorological Society Section: Monthly Weather Review.

Schreck, C. J., J. Molinari, and K. I. Mohr, 2011: Attributing Tropical Cyclogenesis to Equatorial Waves in the Western North Pacific. *Journal of the Atmospheric Sciences*, **68 (2)**,

195–209, doi:10.1175/2010JAS3396.1, URL https://journals.ametsoc.org/jas/article/68/2/195/26740/Attributing-Tropical-Cyclogenesis-to-Equatorial.

Serra, Y. L., G. N. Kiladis, and K. I. Hodges, 2010: Tracking and Mean Structure of Easterly Waves over the Intra-Americas Sea. *Journal of Climate*, **23 (18)**, 4823–4840, doi:10.1175/2010JCLI3223.1, URL https://journals.ametsoc.org/jcli/article/23/18/4823/32596/Tracking-and-Mean-Structure-of-Easterly-Waves-over.

Thorncroft, C., and K. Hodges, 2001: African Easterly Wave Variability and Its Relationship to Atlantic Tropical Cyclone Activity. *Journal of Climate*, **14**, 14.

Torres, V. M., C. D. Thorncroft, and N. M. J. Hall, 2021: Genesis of Easterly Waves over the Tropical Eastern Pacific and the Intra-Americas Sea. *Journal of the Atmospheric Sciences*, **78 (10)**, 3263–3279, doi:10.1175/JAS-D-20-0389.1, URL https://journals.ametsoc.org/view/journals/atsc/aop/JAS-D-20-0389.1/JAS-D-20-0389.1.xml, publisher: American Meteorological Society Section: Journal of the Atmospheric Sciences.

Ullrich, P. A., and C. M. Zarzycki, 2017: TempestExtremes: a framework for scale-insensitive pointwise feature tracking on unstructured grids. *Geosci. Model Dev.*, **10 (3)**, 1069–1090, doi:10.5194/gmd-10-1069-2017, URL https://gmd.copernicus.org/articles/10/1069/2017/.

Ventrice, M. J., and C. D. Thorncroft, 2013: The Role of Convectively Coupled Atmospheric Kelvin Waves on African Easterly Wave Activity. *Monthly Weather Review*, **141 (6)**, 1910–1924, doi:10.1175/MWR-D-12-00147.1, URL https://journals.ametsoc.org/view/journals/mwre/141/6/mwr-d-12-00147.1.xml, publisher: American Meteorological Society Section: Monthly Weather Review.

Wheeler, M., and G. N. Kiladis, 1999: Convectively Coupled Equatorial Waves: Analysis of Clouds and Temperature in the Wavenumber–Frequency Domain. *Journal of the Atmospheric Sciences*, **56 (3)**, 374–399, doi:10.1175/1520-0469(1999)056⟨0374:CCEWAO⟩2.0.CO;2, URL https://journals.ametsoc.org/view/journals/atsc/56/3/1520-0469_1999_056_0374_ccewao_2.0.co_2.xml, publisher: American Meteorological Society Section: Journal of the Atmospheric Sciences.

Chapter A

Density Plots with TC Tracks Included

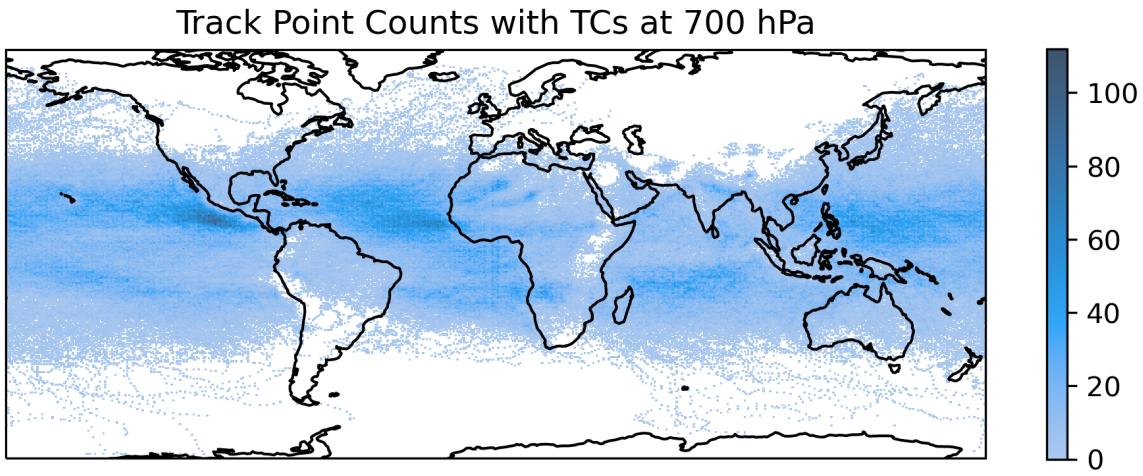

Figure A.1: Number of TEW track points per 0.625°x0.5° grid box, before removing TCs, accumulated over the years 1981-2018, at 700 hPa.

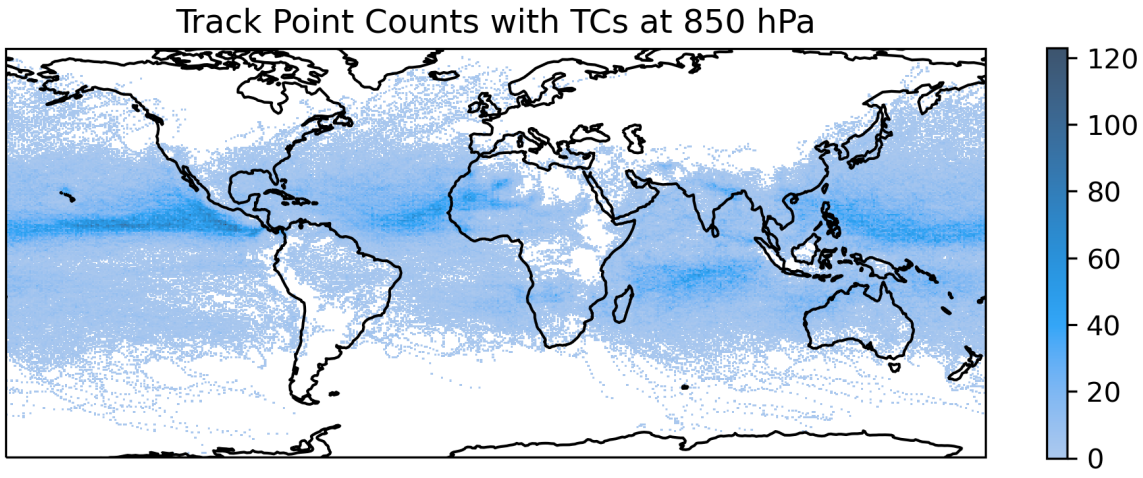

Figure A.2: As Figure A.1 but for 850 hPa.

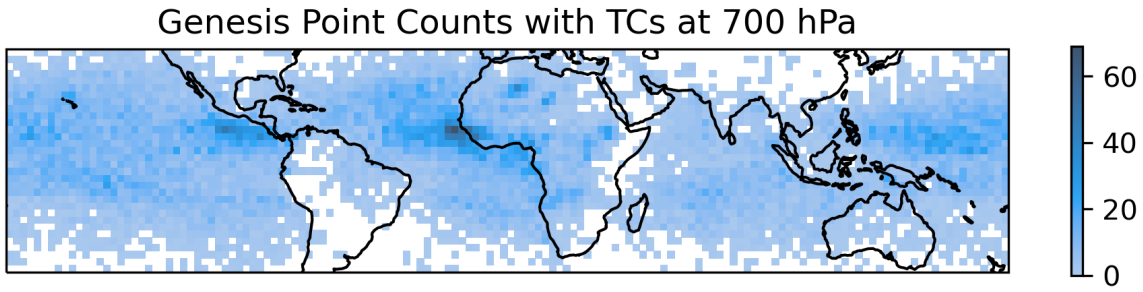

Figure A.3: Number of first points in TEW tracks per 2.5°x2.5° grid box, before removing TCs, accumulated over the years 1981-2018, at 700 hPa

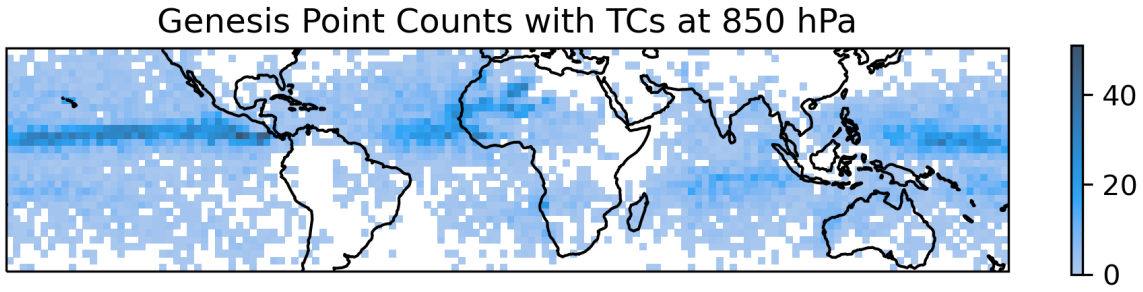

Figure A.4: As Figure A.3 but for 850 hPa.

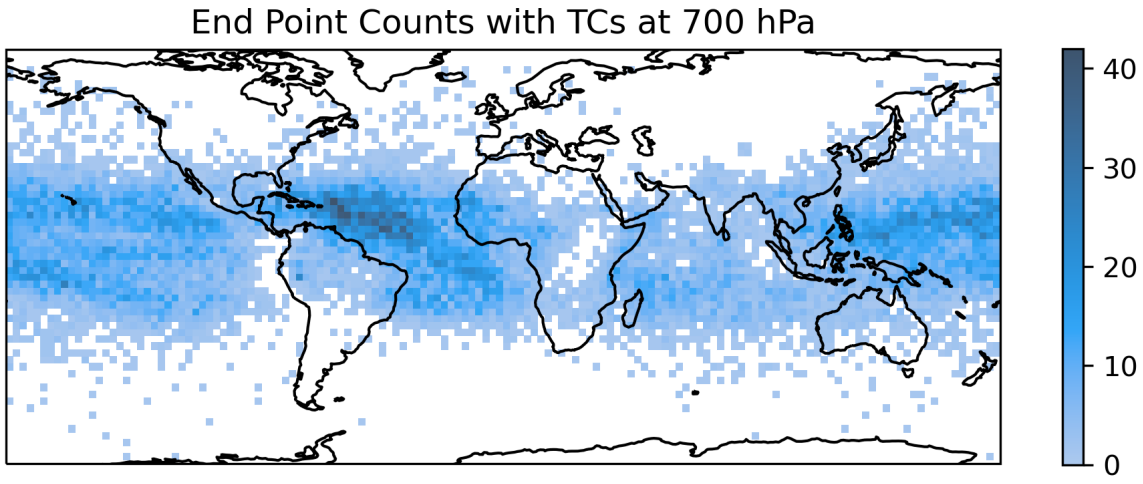

Figure A.5: Number of last points in TEW tracks per 2.5°x2.5° grid box, before removing TCs, accumulated over the years 1981-2018, at 700 hPa

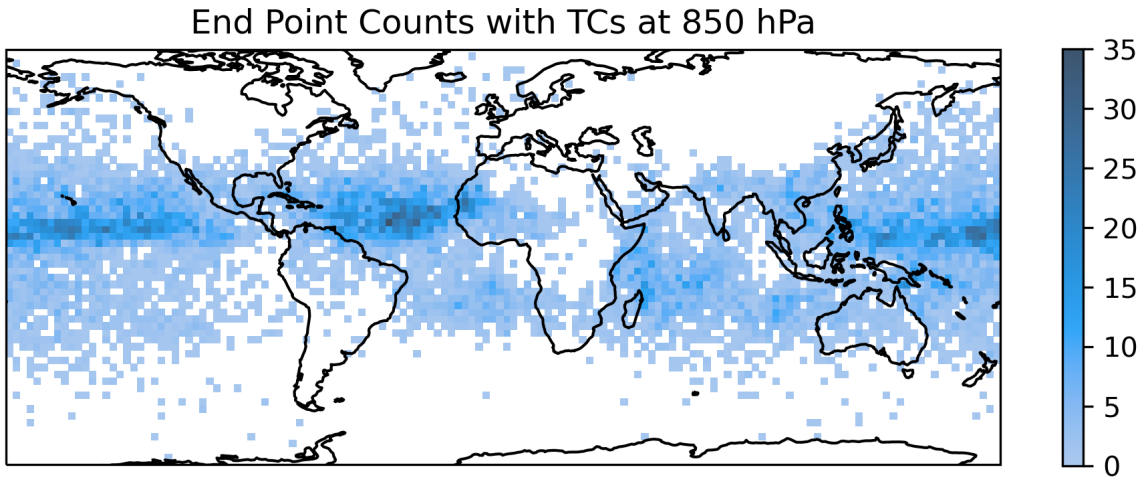

Figure A.6: As Figure A.5 but for 850 hPa.